Quantitative evaluation of radiation change and vegetation recovery during and after fires in tropical peatland

熱帯泥炭地における火災による放射環境の変化と火災後の植生回復の定量的評価

Hokkaido University　Graduate School of Agriculture

Division of Environmental Resources　Doctor Course

Fiolenta Marpaung

Advisor : Prof. Dr. Agr. Takashi Hirano
Co-advisors : Prof. Dr. Agr. Ryoji Sameshima
: Tomomichi Kato, Ph.D.

Date of Oral Examination : 05.08.2016
Date of Approval : 02.09.2016

Abstract

In Southeast Asia, a huge amount of peat has accumulated under peat swamp forest. However, large-scale fires because of land clearing under a dry condition have rapidly devastated these peatlands. El Niño events prolong the dry season and raise the risk of large-scale peat fires by lowering groundwater levels (GWL). Through the fires, biomass and surface peat are burnt and consequently dense smoke or aerosol covers the ground. As a result, solar radiation itself and its ground reflectance are changed. The change of solar radiation both in quantity and in quality affects vegetation photosynthesis. In addition, the change of reflection properties can be used to estimate the vegetation damage and recovery during and after fires. However, knowledge about the effects of peat fires on dynamical surface radiation change is quite limited. Thus, the objectives of this study are to quantitatively evaluate solar radiation change and vegetation recovery during and after the peat fire of 2009 in tropical peatland using long-term monitoring data of radiation, which were measured for more than 10 years (2004-2014) in an ex-tropical peat forest in Central Kalimantan, Indonesia.

1. Environmental dependence and seasonal variation of diffuse radiation in tropical peatland

Daily diffuse fraction (R_d/R_g) of solar radiation was significantly related to the clearness index (R_g/R_o) via a linear threshold model. Under the clear sky, R_d/R_g was larger in tropical peatland with a humid climate than in Australia. Using the model, long-term variation in R_d/R_g was estimated from global solar radiation (R_g). As a result, R_d/R_g showed a seasonal variation with its minimum of 0.51 in June (the transition between the wet and dry seasons) and its maximum of 0.68 in October (the late dry season) on a monthly basis. The decreasing pattern during the transition season

corresponded to decreasing precipitation due to fewer clouds. In contrast, the increasing pattern during the dry season was due to shading by smoke emitted through biomass burning and peat fires. In particular, during the El Niño droughts in 2002, 2006 and 2009, the monthly mean R_d/R_g rose above 0.72, because the ground was densely covered with smoke from large-scale fires.

2. Spectral vegetation dynamics and vegetation recovery in a fire-disturbed ex-tropical peat swamp forest

Vegetation indices (VIs: NDVI and EVI2) and leaf area index (LAI) were derived from spectral reflectance data measured using satellites (MODIS) or tower radiometers to evaluate vegetation recovery after fires. To calculate VIs and LAI, global solar radiation (R_g) has to be separated into photosynthetically active radiation (PAR) and near infrared radiation (NIR). Although the ratio of PAR to R_g tended to increase with the solar zenith angle, the ratio was almost constant at 0.55 at around midday regardless of R_d/R_g. This result improved a model to estimate canopy transmission and surface reflectance of solar radiation. After excluding data under dense smoke from fires, LAI varied seasonally; it decreased as the ground was flooded (GWL $\geq$ 0 m) and increased as GWL lowered underground. Before the fire of 2009, LAI increased up to about 1.5 m^2 m^{-2} according to vegetation recovery after the fire of 2002 with the seasonal variation. The 2009 fire drastically decreased LAI, and then LAI increased year by year. Unlike the LAI, tower-based VIs showed a decreasing tendency in flooded conditions, because NIR reflectance decreased. Even after excluding data under the conditions of dense smoke and flooding, the tower-based VIs showed a different trend from MODIS-based VIs. The MODIS VIs were once decreased by the 2009 fire, and then increased according to vegetation recovery similarly with LAI, whereas tower VIs showed no decrease in 2009. This unexpected trend of tower VIs was probably caused by increased NIR reflectance due to the changed of peat bulk density because of the fire. Further field studies are needed to extract vegetation information from tower VIs by excluding the fire effect on NIR reflectance of the peat surface.

Preface

The presented thesis is written as a cumulative Ph.D thesis. Chapters 2 and 3 are independent papers that have been submitted and/or will be submitted for publication in scientific journals. A general introduction and a concluding chapter with an integrating discussion (Chapter 4) create the necessary frame for joint consideration of the different chapters. To facilitate reading of the thesis, tables and figures were always inserted into the text and formatted in the same way, and font size, line spacing, and captions were adjusted to one format. Enumeration of tables and figures was conducted separately for each chapter.

Contents

List of Symbols

Nomenclature

Latin Letters

A_j	coefficient of diffuse fraction model j = 0 for intercept of linear regression j = 1 for coefficient of linear regression	dimensionless
f_j	radiation intercepted by the canopy j = b for direct radiation j = d for diffuse radiation	dimensionless
$k_{be}(\phi)$	extinction coefficient of a canopy of black leaves with an ellipsoidal leaf angle distribution for direct (beam) radiation	dimensionless
k_d	extinction coefficient of a canopy of black leaves for diffuse radiation	dimensionless
m	optical air mass	dimensionless
L_t	plant height	m
P	actual air pressure	hPa
P_o	sea level pressure constant	1013.25 hPa

P/P_o	ratio of actual to sea level pressure	dimensionless
R_j	solar irradiance (flux density)	W m^{-2} or MJ m^{-2} d^{-1}
	j = a for atmospheric (long-wave) solar irradiance	
	j = b for direct (beam) solar irradiance	
	j = d for diffuse solar irradiance	
	j = DV for potential direct (beam) solar irradiance in visible (PAR) component	
	j = dV for potential diffuse solar irradiance in visible (PAR) component	
	j = DN for potential direct (beam) solar irradiance in near infrared component	
	j = dN for potential diffuse solar irradiance in near infrared component	
	j = g for total solar irradiance	
	j = V for estimated solar irradiance in visible (PAR) component	
	j = N for estimated solar irradiance in near infrared component	
	j = T for estimated total solar irradiance	
	j = o for extra-terrestrial solar irradiance	
R_d/R_g	diffuse fractions	dimensionless
R_g/R_o	clearness index or atmospheric transmission	dimensionless
R_{VIS}	reflectance in the visible wavelength derived from the tower	dimensionless
R_{NIR}	reflectance in the near infrared wavelength derived the tower	dimensionless
VIS_{in}	incident solar irradiance in visible (PAR) component	W m^{-2}
NIR_{in}	incident solar irradiance in near infrared component	W m^{-2}

S_{sc}	solar irradiance constant		1370 W m^{-2}
$S_{sc\text{-}UV}$	solar irradiance constant, excluding ultra violet		1320 W m^{-2}
t_j	time		
	j = d	for day of year	1 – 365 (366)
	j = h	for solar time	h
	j = l	for local time	h
x	the ratio of average projected areas of canopy elements on horizontal and vertical surfaces		dimensionless
X_j	initial threshold of diffuse fraction model x-axis		dimensionless
	j = 0	for intersecting the regression line at the constant values of Y_o	
	j = 1	for intersecting the regression line at the constant values of Y_1	
Y_j	initial threshold of diffuse fraction model in y-axis		dimensionless
	j = 0	for averaged R_d/R_g when R_g/R_o is less than 0.2	
	j = 1	for the minimum value of R_d/R_g	

Greek Letters

α	leaf absorptivity		dimensionless
$\alpha_{j,cpy}$	flux density of the VIS light absorbed by the canopy		W m^{-2}
	j = b, (ϕ)	for direct radiation at zenith angle (ϕ)	
	j = d	for diffuse radiation	
β	solar elevation		° deg.
λ_j	coordinate of the site		° deg.

	j = v for latitude	
	j = h for longitude	
	j = o for local standard time meridian	
δ	solar declination	° deg.
ϖ	time correction factor	min
θ	equation of time	min
φ	day angle	° deg.
η	ratio of the PAR to solar radiation	dimensionless
ϕ	solar zenith angle	° deg.
ω	water absorption in the near infra-red	dimensionless
ρ_j	surface reflectance	dimensionless
	j = red for red wavelength	
	j = NIR for near infrared wavelength	
$\rho^H_{j,cpy}$	the canopy hemispherical reflection coefficient of a green light in closed canopies	dimensionless
	j = b for direct radiation	
	j = d for diffuse radiation	
$\rho^*_{j,cpy}$	reflection coefficient for dense canopies	dimensionless
	j = b, (ϕ) for direct radiation at zenith angle (ϕ)	
	j = d for diffuse radiation	
$\rho_{j,cpy}$	reflection coefficient for sparse canopies	dimensionless
	j = b, (ϕ) for direct radiation at zenith angle (ϕ)	
	j = d for diffuse radiation	
ρ_s	soil reflectivity as the averaged from dry and wet bare ground	dimensionless

$\tau_{j,cpy}$	flux density of VIS light under the sparse canopy	W m^{-2}
	j = b, (ϕ) for direct radiation at zenith angle (ϕ)	
	j = d for diffuse radiation	
τ_j	fraction of VIS light transmitted by a canopy	dimensionless
	j = b, (ϕ) for direct radiation at zenith angle (ϕ)	
	j = d for diffuse radiation	

Abbreviations

ABC	Atmospheric Brown Cloud
AICc	Corrected Akaike Information Criterion
AVHRR	Advanced Very High Resolution Radiometer
CO_2	Carbon Dioxide
CWD	Coarse Woody Debris
DB	Drained Burnt Forest Site
DF	Drained Swamp Forest Site
DOY	Day of Year
EVI	Enhanced Vegetation Index
GPP	Gross Primary Production
GWL	Groundwater Levels (m)
LAI	Leaf Area Index (m^2 m^{-2})
LANDSAT	Land Remote Sensing Satellite

LUE	Light Use Efficiency	
MODIS	Moderate Resolution Imaging Spectroradiometer	
MRP	Mega Rice Project	
NASA	National Aeronautics and Space Administration	
NDVI	Normalized Difference Vegetation Index	
NEE	Net Ecosystem Exchange	
NIR	Near Infra Red	
NIR_{est}	Estimated solar radiation in NIR wavelength	$W\ m^{-2}$
PAI	Plant Area Index	$m^2\ m^{-2}$
PAR	Photosynthetically Active Radiation	$W\ m^{-2}$
PPFD	Photosynthetic Photon Flux Density	$\mu m\ m^{-2}\ s^{-1}$
RMSE	Root Mean Square Error	
SWC	Volumetric Soil Water Content	$m^3\ m^{-3}$
UV	Ultra Violet	
VIs	Vegetation Indices	
VIS	Visible	
VPD	Water Vapor Pressure Deficit	hPa

Chapter 1

Introductions

Peatland is the wetland with a thick waterlogged organic soil layer (peat), which is made up from dead and decaying plants materials. It stores carbon up to 88.6 Pg and contributes about 15-19% of the global carbon pool (Page *et al.*, 2011) in Southeast Asia. However, these peatlands are now being subjected to intensive land use change and conversion into the different forms of agriculture use, including commercial plantations. This is well advanced in Indonesia and Malaysia, where most of the peatland areas have already been deforested, drained, and converted by often using fire as a land clearance tool. Through these processes, the steadily emitted CO_2 through less photosynthesis, and the densely released smoke or aerosol particles would change atmospheric compositions, surface radiation balance, and hence have an effect on the vegetation regrowth. However, only a few studies with short continuous observation in this tropical region exist. Thus, detailed analysis of dynamical surface radiation change and its effect on plant canopy reflectance are needed.

The goal of this thesis is to provide quantitative estimates about the impact of different natural and forest fires factors on radiation in tropical peatland. Underlying physical mechanism for this radiation will be investigated to quantify vegetation recovery on this ecosystem.

1.1. Diffuse radiations in the tropical peatlands

The total or global solar radiation reaching the Earth's surface has two components, i.e. direct beam and diffuse radiation. The direct beam radiation comes in a direct line from the sun, whereas the diffuse radiation is scattered out of the direct beam by aerosols, clouds, air mass, and water vapor concentration. These atmospheric conditions (porous media) increase the proportion of diffuse radiation in global solar radiation. The spectral portion of the solar spectrum (i.e. PAR – Photosynthetically Active Radiation) is the primary driver of plants photosynthesis. Leaf photosynthesis increases non-linearly with incident PAR when other environmental variables are not limited. However, besides the intensity, the geometry of PAR is also important in plant canopies. Leaves at lower level receive periods of bright light depending on the solar trajectory and the movement of leaves by winds. In addition, the photosynthesis is greater if two leaves receive the moderate PAR than if one leaf receives excessive PAR while the other in the shade. Therefore, the uniform distributions of PAR in plant canopies are important, with uncertain overall effects on global plant productivity and the land carbon sink (Farquhar and Roderick, 2003; Kanniah *et al.*, 2012; Mercado *et al.*, 2009).

Under a clear sky condition, a fraction of the plant canopy is illuminated by direct solar radiation with the remaining portion of the canopy being in the shade. The sunlit fraction of the canopy has leaves that are often light saturated, and therefore have a low light-use efficiency (LUE), whereas leaves in the shade have a high LUE but receives much less PAR (Mercado *et al.*, 2009). In contrast, under cloudy or hazy conditions, sunlight is more scattered, and global solar radiation received at the surface is attenuated with a high diffuse fraction. The diffuse PAR produces a more uniform irradiance, and penetrates deeper into the light-limited lower canopy, reducing the

photosynthetic saturation and enhancing LUE. As a result, canopy photosynthesis leads to be significantly more LUE under diffuse radiation than direct radiation (Gu *et al.*, 2002; Knohl and Baldocchi, 2008; Roderick *et al.*, 2001; Still *et al.*, 2009; Zhang *et al.*, 2011). Moreover, enhancing intermediate levels of diffuse PAR fraction, such as thin or scattered clouds or higher aerosol concentration from volcanic eruptions or anthropogenic emissions, will have a positive outcome to the annual gross primary production (GPP), while an increase in cloud cover will have a negative impact (Oliphant *et al.*, 2011). Therefore, studying the effects of diffuse PAR on ecosystem productivity has become one of the main goals in terrestrial carbon cycle researchers (Hirano *et al.*, 2012; Knohl and Baldocchi, 2008; Matsui *et al.*, 2008; Oliveira *et al.*, 2007; Still *et al.*, 2009; Suzaki *et al.*, 2003).

The ratio of PAR and global solar radiation depends on the extent to which it is independent of solar altitude, atmospheric composition, and cloud conditions. Observational and experimental evidences show that in the higher and middle latitudes, daily averages of the ratio is less affected by atmospheric and sky conditions, whereas, in the tropics, the ratio is strongly affected by atmospheric conditions, especially cloudy conditions (Spitters, 1986; Spitters et al., 1986; Weiss and Norman, 1985) . For this thesis, the couplings of PAR with diffuse radiation because of fire disturbances in tropical peat swamp forest are investigated. More details about diffuse radiation, what are the environmental dependencies and the disturbance factors that affect its seasonal variations; can be found in Chapter 2, whereas a detailed evaluation of the ratio of PAR can be found in Chapter 3.

1.2. Monitoring vegetation regrowth

Deforestation and tropical swamp forest fires switch the tropical peatland from being a carbon sink to become a carbon source (Sorensen, 1993). These disturbances affect the ecosystem, changing the energy and water balance, and also altering the atmospheric water content and precipitation patterns (Putra and Hayasaka, 2011). Moreover, deforestation in this region has the potential to lead to serious global consequences because the peat swamp forest ecosystems host exceptionally high biodiversity and immense amounts of carbon (Miettinen *et al.*, 2011). Disturbance events like forest fire cause changes in the spatial heterogeneity of landscape mosaic, which is important for ecosystem process, and management affects biodiversity as the landscape adapts to and recovers from repeated forest fire events. Thus, they generally affect vegetation regrowth across a range of burning severity.

The degree of vegetation recovery after fire depends on the time from the previous fire (Tessler *et al.*, 2015), burning season (Pavlovic *et al.*, 2011), and climate and post-fire weather conditions (Knox and Clarke, 2006; Konstantinidis *et al.*, 2006). It also depends on fire severity (Diffendorfer *et al.*, 2012; Hoscilo *et al.*, 2013, 2011; Kuenzi *et al.*, 2008; Vivian *et al.*, 2008) which will change the condition of type and amount of nutrients that are available (Pereira *et al.*, 2012). Low-severity fires do not have strong environmental impacts, whereas severe fires give negative impacts, such as reduction of soil organic matter, degradation of soil structure and aggregation (Jordán *et al.*, 2011; Mataix-solera *et al.*, 2011), and change in hydrological response (Granged *et al.*, 2011).

Remote-sensing technologies have been widely used to assess and map the effects of fire on vegetation conditions and subsequent to vegetation recovery trends over time. It also allows us to monitor land surface phenology or the timing of

vegetation growth stages, particularly by land surface characteristics, which are relevant to vegetation indices (VIs) and leaf area index (LAI). For example, the Normalize Difference Vegetation Index (NDVI; Tucker, 1979) and Enhanced Vegetation Index (EVI/ EVI2; (Jiang *et al.*, 2008; Verstraete and Pinty, 1996) that are derived from high temporal frequency reflectance data of the heritage Advanced Very High Resolution Radiometer (AVHRR), the current NASA Moderate Resolution Imaging Spectroradiometer (MODIS), Land Remote Sensing Satellite (LANDSAT), spectrometer, or the micrometeorological radiations sensor (Huemmrich *et al.*, 1999; Wilson and Meyers, 2007). These are the most commonly vegetation indices used for local, regional and continental studies and, they are sensitive to absorbed PAR, greenness and GPP when integrated over the season (Myneni *et al.*, 1997; Tucker and Sellers, 1986; Turner *et al.*, 2004). However, little information is available about vegetation recovery and LAI in tropical peatland that was severely damaged by fire. The satellite data can be difficult to be processed and still contain occasional spurious inferences due to aerosol, cloud cover, and the surface bidirectional reflectance distribution (BDRF) (Berk *et al.*, 1998; Disney *et al.*, 2004; Nagai *et al.*, 2009), especially in the tropics. The broadband VIs from the micrometeorological radiation sensors also might contain spurious interferences from the coupling of PAR with diffuse radiation (Chapter 2), whereupon both processes lead to change in albedo, surface reflectance, and intercepted radiation within the canopies. The use of surface reflectance– diffuse radiation allows performing a sensitivity study, particularly analysis of LAI within sparse canopies. More details about the spectral vegetation dynamics, vegetation regrowth, and how peat fires and other environmental factors influence them in tropical peatland are described in Chapter 3.

1.3. Scientific questions of this thesis

This thesis investigates the influence of different natural and forest fires factors on the dynamical diffuse radiation in the tropical peatland. Further analyses of this radiation are done and then used to determinate canopy reflectance and quantify vegetation recovery. The following questions are addressed in the coming chapters, which are all reprints of publications accepted in or will be submitted to scientific journals.

- **How does the forest fires influence diffuse radiation in the tropical peat swamp forest – what is the diffuse fraction profile in tropical peatland?** (Chapter 2)
- **How does severe fire affect the spectral component of solar radiation in tropical peatland?** (Chapter 3)
- **How does the surface reflectance change after forest fire in the tropical peat swamp forest – How is the vegetation recovery after fire in this ecosystem?** (Chapter 3)

To answer these questions, a continuous measurement of diffuse radiation has been performed for more than three years, and the model output for long-term monitoring has been analyzed in tropical peatland. The model that is performed and analyzed here is unique, considering that it consists of various long-term atmospheric conditions (up to 14 years) measurements. The model stand-alone has been previously evaluated and has been found to exhibit a realistic diffuse fraction and the spectral portion of solar components (Roderick [1999] and Stigter and Musabilha [1982], respectively). The model was then applied as the independent parameter of micrometeorological tower data to access canopy reflectance and investigate vegetation

recovery. Details of the model and the estimation of spectral vegetation dynamics are described in the respective chapters of this thesis.

Chapter 2

Environmental dependence and seasonal variation of diffuse radiation in tropical peatland

Different natural and anthropogenic factors can have an influence on solar radiation as has been introduced in the previous chapter. Besides this general influence, these factors might also affect the "extreme events" in this region, which are diffuse radiation induced by forest fires. In this chapter, which is a reprint of an article of the same title published in Journal of Agricultural Meteorology, the environmental dependencies on diffuse radiation, modeling of diffuse radiation for long-term monitoring, and the seasonal variability are investigated.

Citation: **Marpaung F, Hirano T 2014: Environmental dependence and seasonal variation of diffuse radiation in tropical peatland. J. Agric. Meteorol., 70, 334–341, doi:10.2480/agrmet.D-14-00028**.

2.1. Introduction

Peatlands are carbon-dense ecosystems that are vulnerable to disturbances through human activities and climate change. In the tropics, peatlands are widely distributed over 4.41×10^5 km^2 (about 11% of global peatland area) and store soil carbon up to 88.6 Pg. (15-19 % of the global peat carbon pool) with 57.4 Pg of carbon stored in Indonesia (Page *et al.*, 2011). However, poor land management practices, such as logging, drainage and fires have disturbed tropical peatlands in Southeast Asia. In Indonesia, peat swamp forests of 2.76×10^4 km^2 were deforested and drained for the last decade (Miettinen *et al.*, 2011). As a result, large amounts of CO_2 have been steadily emitted through less photosynthesis and more oxidative peat decomposition (Couwenberg *et al.*, 2010; Hirano *et al.*, 2014; Hooijer *et al.*, 2010). The fires are often triggered by lower groundwater level (Putra and Hayasaka, 2011; Putra *et al.*, 2008) and land clearing (Murdiyarso and Adiningsih, 2007) in the late dry season, especially during El Niño drought. Large-scale peat fires occurred in Sumatra and Central Kalimantan, Indonesia, in El Niño years of 1997, 2002, 2006, and 2009 (Ballhorn *et al.*, 2009; Langner and Siegert, 2009; Page *et al.*, 2002; Tosca *et al.*, 2011; van der Werf *et al.*, 2008). Smoke and aerosol released to the atmosphere during peat fires attenuate global solar radiation (R_g) and increase fraction of diffuse solar radiation (R_d/R_g) on the ground. Increased diffuse radiation produces more uniform irradiance with smaller fractions of light-saturated leaves and penetrates deeper into the light-limited lower canopy, which results in an increase in the light-use efficiency of gross primary production (GPP) (Gu *et al.*, 2002; Knohl and Baldocchi, 2008; Oliphant *et al.*, 2011).

Some studies examined the effects of aerosol and clouds on radiation and their impacts on canopy gas exchange processes in temperate forests (Knohl and Baldocchi, 2008; Matsui *et al.*, 2008; Still *et al.*, 2009; Suzaki *et al.*, 2003) and tropical forests

(Oliveira *et al.*, 2007). For tropical peat swamp forest, Hirano *et al.* (2012) simply examined the effect of smoke from peat fires in 2006 on GPP using the light curve of GPP and the clearness index (R_g/R_o): the ratio of R_g and extra-terrestrial solar radiation (R_o), as an index of the fraction of the diffuse radiation (R_d) (Roderick, 1999; Spitters *et al.*, 1986). However, field information on R_d in tropical peatland, where are periodically covered by dense smoke through peat fires in response to El Niño drought, is quite limited.

Therefore, we continuously measured R_d along with other environmental elements in tropical peatland in Central Kalimantan, Indonesia for more than three years. Using the field data, we analyzed the relationships between R_d/R_g and environmental factors and parameterized a linear threshold model (Roderick, 1999) to estimate R_d/R_g from R_g/R_o. Moreover, we examined seasonal variation in the radiation environment of tropical peatlands and the effect of smoke due to biomass burning and peat fires on R_d/R_g using long-term data of R_g from 2001 to 2013.

2.2. Material and methods

2.2.1. Site description

The study was carried out at two sites (DF and DB) on tropical peatland in Central Kalimantan province, Indonesia. The sites were about 15 km apart from Palangkaraya, the capital of the province (Hirano *et al.*, 2012). The DF site (2°20′45.9″S, 114°2′11.1″E) with a 50-m-high tower was located in a secondary forest remaining in Block C of the Mega Rice Project (MRP): a national project of peatland conversion into rice fields during the late 1990s. The DB site (2°20′26.9″S, 114°2′16.4″E) with a 4-m-high tower was located in an ex-forest, which was burnt three times during El Niño drought in 1997, 2002 and 2009. The two sites were about 600 m away from each other.

A large canal (25 m wide, 3.5 - 4.5 m deep), which was excavated in 1996 and 1997, runs between the two sites and has functioned effectively to facilitate drainage. The sites are described in detail by Hirano *et al.* (2012).

Annual precipitation and annual mean air temperature from 2002 to 2009 were 2452 mm yr^{-1} and 26.1°C, respectively (Hirano *et al.*, 2012). Although air temperature is mostly constant throughout a year, precipitation shows clear seasonality. According to a precipitation threshold of 100 mm $month^{-1}$ (e.g. Oldeman *et al.*, 1980), the dry season occurs for three to five months from June to October on average (Hirano *et al.*, 2007; Putra and Hayasaka, 2011), owing to the strong influence of the dry southeast monsoon (Aldrian and Dwi Susanto, 2003). An El Niño event prolongs the dry season and raises the risk of large-scale peat fires by lowering groundwater levels (GWL). El Niño drought occurred in 2002, 2006 and 2009 (Hirano *et al.*, 2012; Putra and Hayasaka, 2011).

2.2.2. Field data

Meteorology and GWL have been measured since July 2001 and April 2004, respectively, at DF and DB. At the both sites, global solar radiation (R_g) and atmospheric radiation or downward long-wave radiation (R_a) were measured above the canopy with a radiometer (CNR-1; Kipp & Zonen, The Netherlands). On the other hand, R_g and diffuse radiation (R_d) were measured with a sunshine sensor (BF3; Delta-T devices, UK) only at DB since March 2010; the data have some gaps due to sensor malfunction. In addition, air temperature, relative humidity, and precipitation have been measured at the heights of 41.7 and 1.5 m, respectively, at DF and DB (Hirano *et al.*, 2012, 2007). Half-hourly means of meteorology and GWL, which were measured at

intervals of 10 or 30 sec, were recorded with a data logger (CR10X; Campbell Scientific Inc., USA).

2.2.3. Data analysis

Diffuse fraction (R_d/R_g) was calculated using outputs from BF3, whereas atmospheric transmission/clearness index (R_g/R_o) was determined from measured R_g with CNR1 and extra-terrestrial solar radiation (R_o) calculated according to Spitters *et al.* (1986), Roderick, (1999), and Khan (2009), because a thermopile sensor (CNR1) is generally more reliable than a photodiode sensor (BF3) for R_g measurement.

The R_o (W m^{-2}) was calculated using the following equations.

$$R_o = S_{sc}\,[1 + 0.033\,cos\,(360t_d/365)]\,sin\beta \tag{2.1}$$

$$sin\beta = sin\lambda_v\,sin\delta + cos\lambda_v\,cos\delta\,cos[15\,(t_h - 12)] \tag{2.2}$$

$$sin\delta = -\sin(23.45°)\,cos[360(t_d + 10)/365] \tag{2.3}$$

$$t_h = t_l + \frac{\varpi}{60} \tag{2.4}$$

$$\omega = 4(\lambda_h - \lambda_o) + \theta \tag{2.5}$$

$$\theta = 9.87\sin(2\varphi) - 7.53\cos(\varphi) - 1.5\sin(\varphi) \tag{2.6}$$

$$\varphi = \frac{360}{365}(t_d - 81) \tag{2.7}$$

where S_{sc} is solar constant (=1370 W m^{-2}), β is solar elevation (deg.), t_d is Day of Year (DOY), λ_v is latitude (deg.), δ is solar declination (deg.), t_h is solar time (h), t_l is local time (h), ϖ is a time correction factor (min), θ is the equation of time (min), λ_h is longitude (deg.), λ_o is the local standard time meridian (deg.) and φ is day angle (deg.).

The R_d/R_g depends on solar altitude and tends to increase as solar altitude declines because of an increase in optical path length. Thus, in half-hourly analysis, data around midday from 1000 to 1400 hours were only used to eliminate the effect of solar altitude. In addition, data during rain and within an hour after a rain event were excluded to minimize the interference from raindrops on the dome of radiometers. In daily and monthly analyses, R_d/R_g was calculated from the sums of all half-hourly data of R_d and R_g in the daytime.

To estimate R_d/R_g for a long period from R_g/R_o, we applied a simple linear threshold model (Roderick, 1999), described as:

$$\frac{R_d}{R_g} = Y_0 \quad for \quad \frac{R_g}{R_o} \leq X_0 \tag{2.8a}$$

$$\frac{R_d}{R_g} = A_0 + A_1 \frac{R_g}{R_o} \quad for \quad X_0 < \frac{R_g}{R_o} \leq X_1 \tag{2.8b}$$

$$\frac{R_d}{R_g} = Y_1 \quad for \quad \frac{R_g}{R_o} \geq X_1 \tag{2.8c}$$

$$A_0 = Y_1 - A_1 X_1 \tag{2.8d}$$

$$A_1 = \frac{Y_1 - Y_0}{X_1 - X_0} \tag{2.8e}$$

where R_d, R_g, and R_o are respective daily totals. The parameters (X_0, X_1, Y_0, Y_1, A_0, and A_1) were determined using the data measured at DB from March 2010 to December 2013. The Y_1 was set equal to the minimum value of R_d/R_g, which was 0.15. The Y_0 was determined by averaging R_d/R_g for days when R_g/R_o was less than 0.2.The A_0 and A_1 were determined by linear regression between R_d/R_g and R_g/R_o when R_g/R_o was larger than 0.25. The X_1 and X_0 were subsequently derived from eq. (2.8d) and (2.8e) (Roderick, 1999). Using the model, long-term R_d/R_g for more than 12 years were assessed from R_g measured at DF.

2.3. Results

2.3.1. Environmental dependence of diffuse fraction

Figure 2.1 shows the relationships of several radiation components with R_d/R_g around midday (1000-1400 h) in rainless conditions at DB. Direct radiation (R_b) was

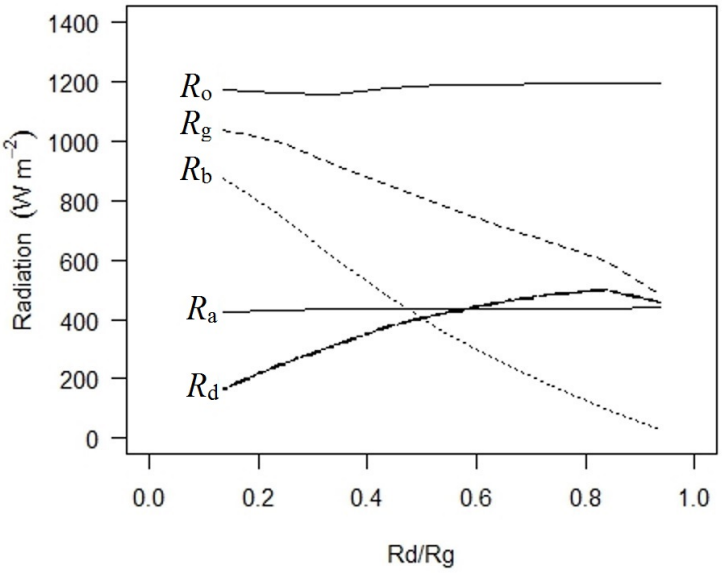

Figure 2.1 Relationships between radiation components (*Ro, Rg, Rb, Ra*, and *Rd*) and the diffuse fraction (*Rd/Rg*) in rainless condition around midday (1000 – 1400 h) from March 2010 to December 2013 at DB site. *Ro* is extra-terrestrial solar radiation, *Rg* is global solar radiation, *Rb* is direct radiation, *Ra* is atmospheric radiation, and Rd is diffuse radiation.

determined as a difference between R_g and R_d, which were measured with BF3. Under a constant value of R_o and R_a, R_g and the R_b (the difference between R_g and R_d) decreased as R_d/R_g increased. The R_d continued to increase with R_d/R_g when the fraction was less than around 0.8. In contrast, above the R_d/R_g of 0.8, R_d decreased, whereas the decreasing rate was smaller than that in R_g. The decrease in R_d along with R_g indicates that R_d/R_g becomes saturated (Fig. 2.2a; the two curves of R_g and R_d would meet at a point of around R_d/R_g of 1.0) in overcast conditions.

To analyze the environmental dependence of R_d/R_g, it was plotted against R_g/R_o, vapor pressure deficit (VPD) at a height of 1.5 m, R_a, groundwater level (GWL), and precipitation on half-hourly and daily basis (only a daily basis for precipitation) using

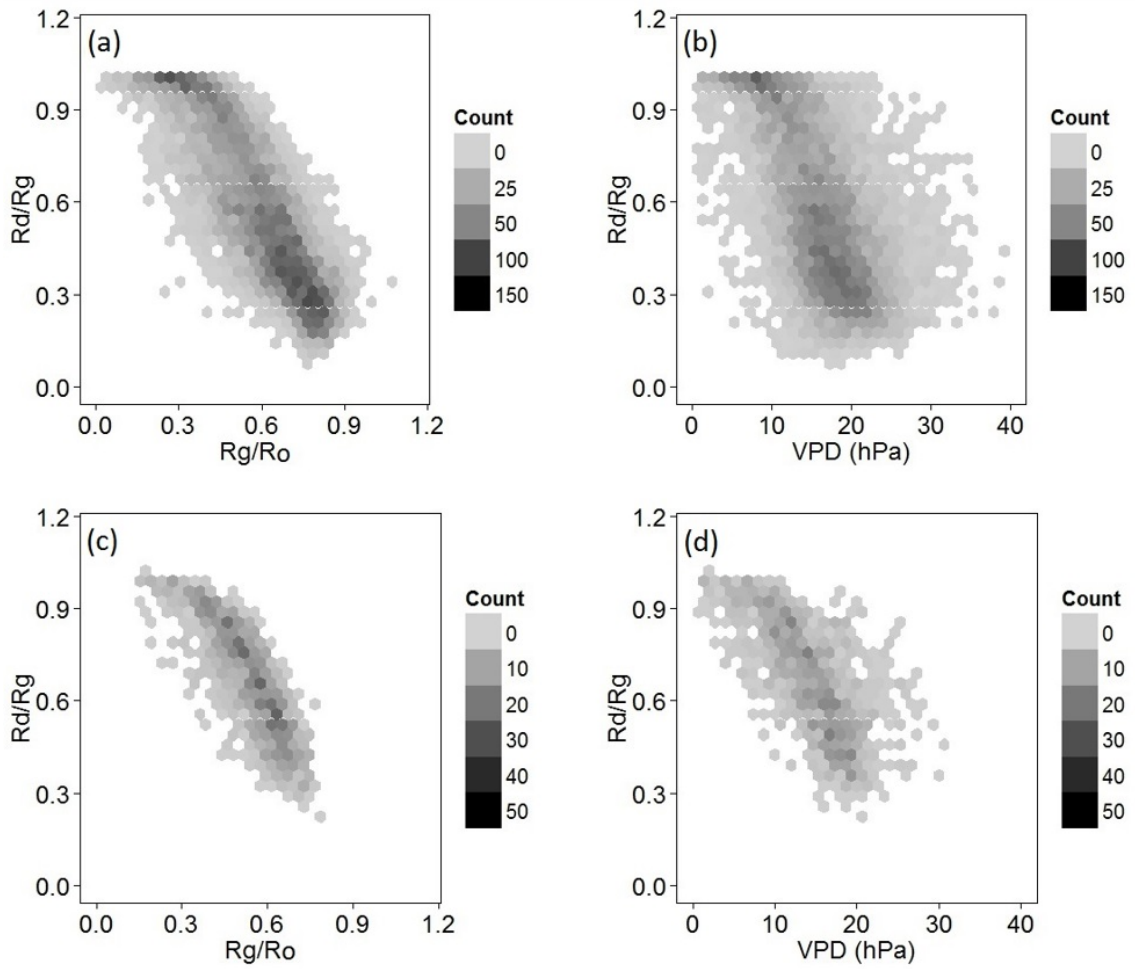

Figure 2.2 Relationships between the diffuse fraction (R_d/R_g) and clearness index (R_g/R_o) or vapor pressure deficit (*VPD*) at DB on half-hourly (a and b) and daily (c and d) bases. For half-hourly relationships, data only in rainless condition around midday (1000 – 1400 h) are used.

DB data. Although no significant correlation was found with R_a, GWL and precipitation ($r^2 < 0.06$) (data are not shown), R_d/R_g showed significant negative linearity ($p < 0.01$) with half-hourly R_g/R_o ($r^2 = 0.71$), daily R_g/R_o ($r^2 = 0.79$), half-hourly VPD ($r^2 = 0.34$), and daily VPD ($r^2 = 0.49$) (Fig. 2.2). The negative relationships indicate that R_d/R_g increases as aerosols and cloud particles increase, and/or the amount of water vapor increases through the enhancement of scattering. The r^2 values were higher on a daily basis for both R_g/R_o and VPD.

2.3.2. Modeling of diffuse fraction

The linear threshold model described as Eq. (2.8) was parameterized on a daily basis and each parameter was determined as X_0 = 0.26, X_1 = 0.84, Y_0 = 0.96, Y_1 = 0.15, A_0 = 1.32 and A_1 = -1.39 (Fig. 2.3). The r^2 value and root mean square error (RMSE) were 0.78 and 0.089, respectively. Simple linear correlation between R_d/R_g and R_g/R_o for

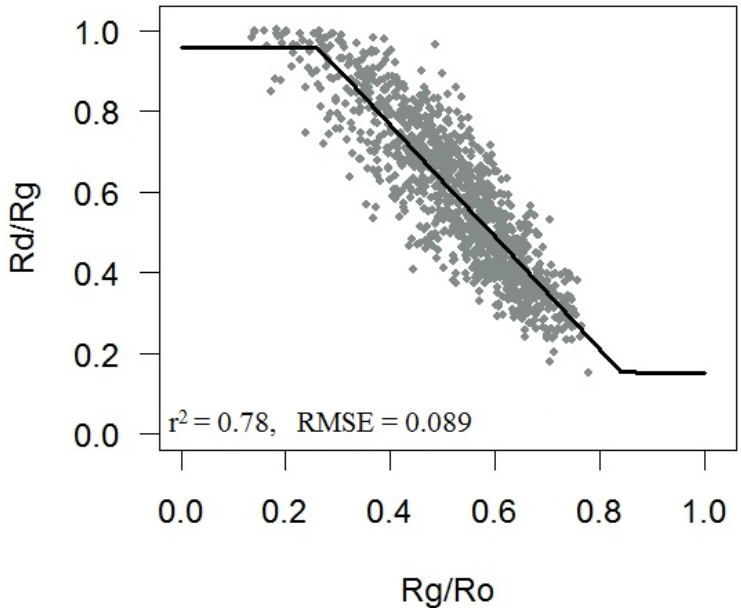

Figure 2.3 Fitting of linear threshold model for the daily relationship between the diffuse fraction (R_d/R_g) and clearness index (R_g/R_o).

all daily data showed r^2 of 0.77 ($p < 0.001$) and RMSE of 0.090, which means that the performance of the linear threshold model is slightly higher than the simple linear relationship. The linear correlation was also significant ($p < 0.001$) even using moving-average data for 5, 10, 15, and 30 days, whereas r^2 decreased from 0.72 to 0.69 as the number of days for averaging increased from 5 to 30 days. This significant linear relationship shows that R_g/R_o is an effective index for R_d/R_g even on a monthly basis (Roderick, 1999).

2.3.3. Seasonal variation in diffuse fraction

The R_g measured with CNR1 was almost identical for DB and DF on a daily basis. Therefore, the linear threshold model parameterized using DB data is applicable to DF. The time sequence of monthly mean R_d/R_g, which were calculated based on daily data, was shown in Fig. 2.4 along with GWL and precipitation for more than 12 years. The R_d/R_g shows a relatively regular cycle with an annual trough; monthly R_d/R_g becomes

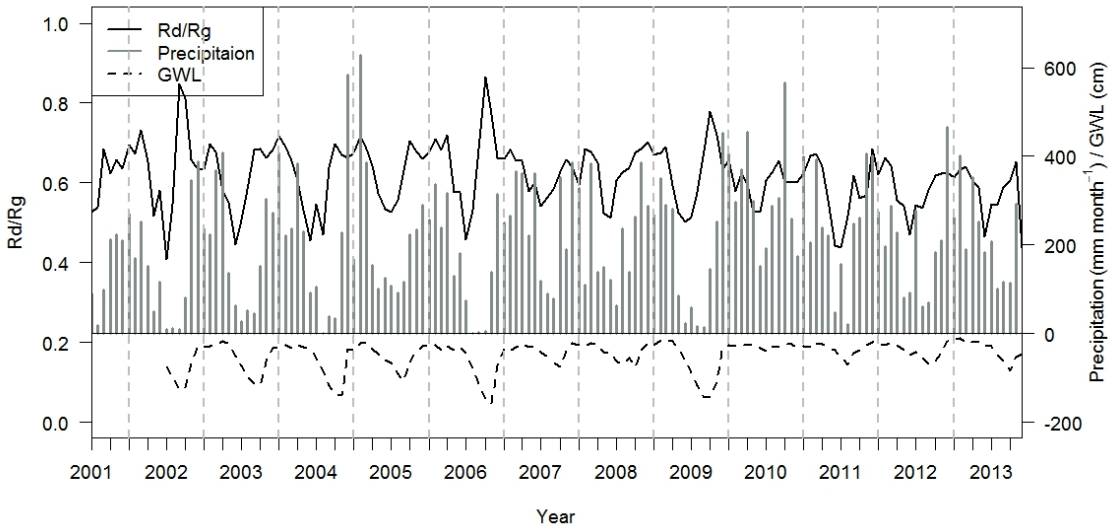

Figure 2.4 Time sequences of monthly values of estimated diffuse fraction (R_d/R_g), precipitation, and groundwater level (*GWL*) at DF site from July 2001 to December 2013.

lower than its mean (0.62) in the early dry season. In addition, R_d/R_g shows sharp peaks above 0.72 in El Niño year of 2002, 2006, and 2009. The peaks correspond to the large drops of GWL caused by El Niño drought.

Monthly data at DF from 2001 to 2013 were ensemble-averaged to clarify seasonal variations (Fig. 2.5). A relatively large standard deviation of R_d/R_g for each month resulted from interannual variations in the seasonality of precipitation and the occurrence of peat fires, which were caused by El Niño and La Niña events. Monthly mean R_d/R_g began to decrease in April and reached its minimum of 0.51-0.52 in June and July, the transition between the wet and dry seasons. This decreasing pattern corresponded to decrease in precipitation and increase in VPD, which reflect decreasing

amount of cloud. During the dry season, monthly R_d/R_g gradually increased and reached its maximum of 0.68 in October, the transition between the dry and wet seasons on average. In October, GWL reached a negative peak of -0.91 m and daytime VPD (0900 to 1500 h) kept the largest level. The increase of R_d/R_g was due to smoke emitted through biomass burning and peat fires, especially during El Niño drought, because precipitation remained low and daytime VPD remained high. Such a dry condition lowers GWL and raises the risk of peat fires (Putra and Hayasaka, 2011). Monthly mean R_d/R_g was lower than its annual mean of 0.62 for four consecutive months from May to August.

2.3.4. Effects of peat fires

Figure 2.6 shows seasonal variations in R_d/R_g estimated from R_g/R_o, R_g, GWL, precipitation and daytime VPD at DB from July 1 (DOY182) to November 30 (DOY334) in 2009 (El Niño year) and 2010 (La Niña year). Sums of precipitation for the five months were 489 and 1633 mm, respectively, in 2009 and 2010, which caused a large interannual difference in daytime VPD; mean daytime VPDs were 19.4 and 12.6 hPa, respectively, in 2009 and 2010. In 2009, GWL remained below -0.25 m throughout the five months. The GWL decreased continuously from July to early October with a negative peak of -1.15 m. In the dry condition, a series of peat fires occurred in August and grew up extensively in September and October (Yulianti *et al.*, 2012). Because dense smoke covered the ground, R_d/R_g continued to increase up to 0.8 between early August and mid-October regardless of fewer clouds, which was judged from a large number of rainless days. On the other hand, in 2010, GWL never lowered underground because of continual precipitation. As a result, no peat fires occurred in the five months, in which the dry season is usually included. Although R_d/R_g remained relatively high

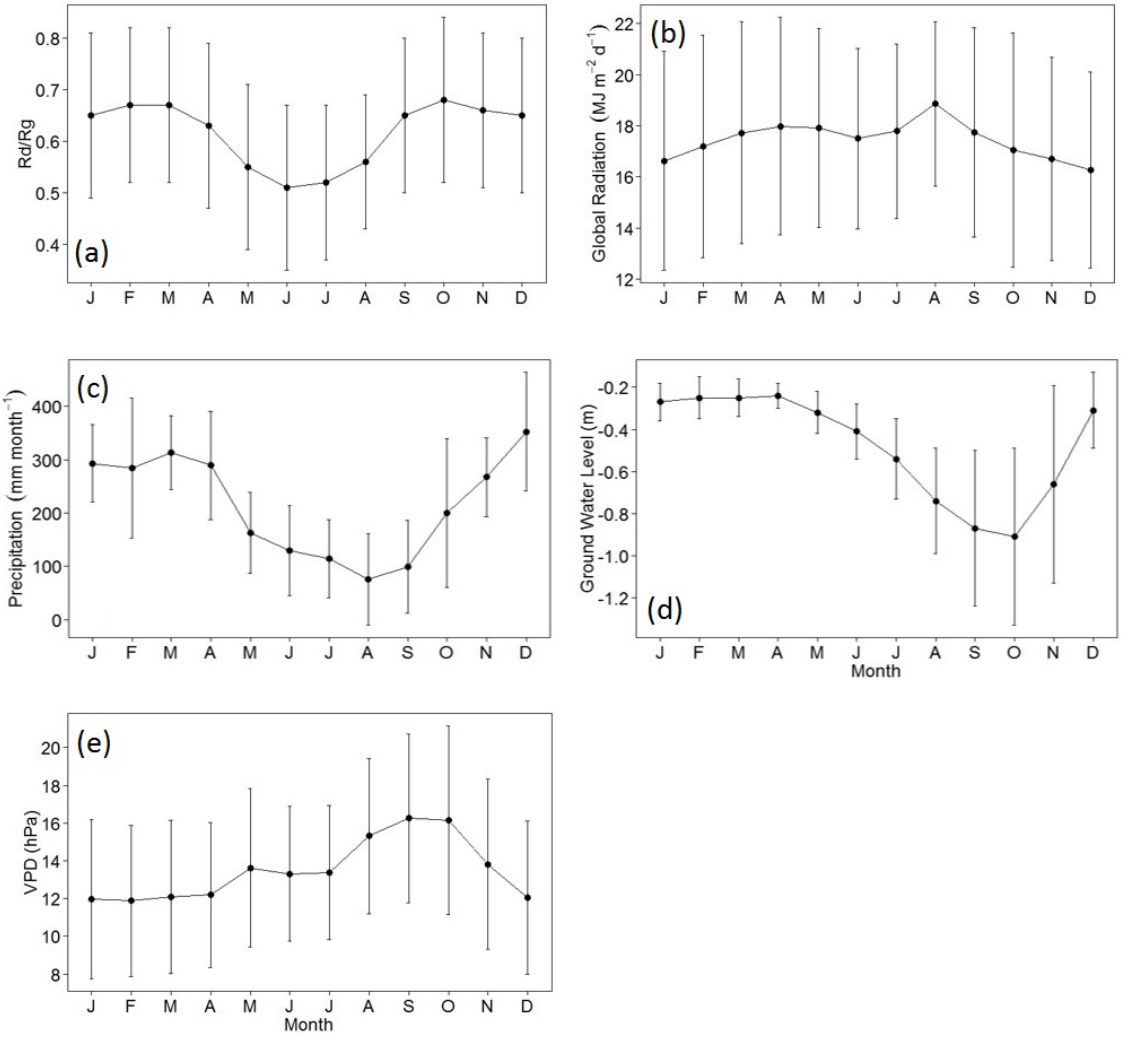

Figure 2.5 Mean seasonal variations in monthly values of the diffuse fraction (R_d/R_g) (a), global solar radiation (R_g) (b), precipitation (c), groundwater level (GWL) (d), daytime vapor pressure deficit (VPD) (0900-1500 h) (e) at DF site for 12 years from 2002 to 2013. Each vertical bar denotes one standard deviation.

during the period because of more clouds in 2010, R_d/R_g in October and November was considerably higher in 2009 than in 2010. In addition, R_g in October and November was lower by 20% in 2009 because of smoke cover.

2.4. Discussion

The linear threshold model (Roderick, 1999) was parameterized for tropical peatland (2.3°S) in Indonesia (Fig. 2.3). The parameters of Y_0 (0.96) and X_0 (0.26),

which stand for the saturated diffuse fraction (R_d/R_g) and the saturation point of clearness index (R_g/R_o), at which R_d/R_g becomes saturated, respectively, were the same as the means for 25 sites in Australia and Antarctica (12.4°S-67.6°S) (Roderick, 1999). The Y_0 of 0.96 suggests that 4% of R_g reaches the ground as beam (R_b) even in overcast conditions. Our results of 0.15 and 0.84 for Y_1 and X_1, respectively, were larger than the means for the 25 sites (Y_1 = 0.05 and X_1 = 0.79) (Roderick, 1999). The Y_1 and X_1 stand for the minimum R_d/R_g and the upper limit of R_g/R_o for linearity with R_d/R_g, respectively. Roderick (1999) reported that X_1 depends on latitude in a quadratic manner. According to his equation, can be calculated to be 0.80 for the latitude of 2.3°S, which is smaller than our result. Therefore, the low value of R_d/R_g was approximated to be 0.15 with extrapolating X_1 for larger R_g/R_o. In addition, larger X_1 indicates larger R_d/R_g at a given R_g/R_o if Y_1 is fixed. Also, larger Y_1 indicates larger R_d/R_g under a clear sky. The larger Y_1 and X_1 for our site than those in Australia is chiefly attributable to the moist atmosphere with more water vapor in tropical rainforest climate that is defined as annual precipitation > 1500 mm yr^{-1} and dry season length < six months (Lewis, 2006).

The R_d/R_g continued to decrease from the late wet season to the early dry season and then increased during the latter half of the dry season (Fig. 2.5). The decreasing pattern was due to decreased cloud amount and higher VPD (Fig. 2.2). Such a seasonal variation in R_d/R_g in accordance with a precipitation pattern was also reported for Amazonian rainforests (Butt *et al.*, 2010). On the other hand, smoke shading due to the burning of biomass and peat also caused the increase in R_d/R_g. In this area of tropical peatland, most of fires are human-caused and occur in the mid- to late dry seasons from August through October (Yulianti *et al.*, 2012). Thus, such human activities emit smoke and increases R_d/R_g even in the dry season with less precipitation. The fires often enlarge extensively during the prolonged dry season due to El Niño drought, and

consequently, massive smoke is emitted through peat burning (Page *et al.*, 2002; Putra and Hayasaka, 2011; Toriyama *et al.*, 2014). Sharp peaks of R_d/R_g in 2002, 2006, and 2009 were caused by dense smoke from large-scale peat fires (Fig. 2.4).

The large R_d/R_g during El Niño drought suggests an increase in the atmospheric density of hygroscopic aerosol, which originated from smoke. The aerosol acts as cloud condensation nuclei and changes the size distribution of cloud particles (Kaufman and Fraser, 1997). Moreover, particles emitted through biomass burning and peat fires in Kalimantan, which had high sulfur content and high hygroscopicity, enlarged the size distribution of cloud particles (Ikegami *et al.*, 2001) and consequently increased the

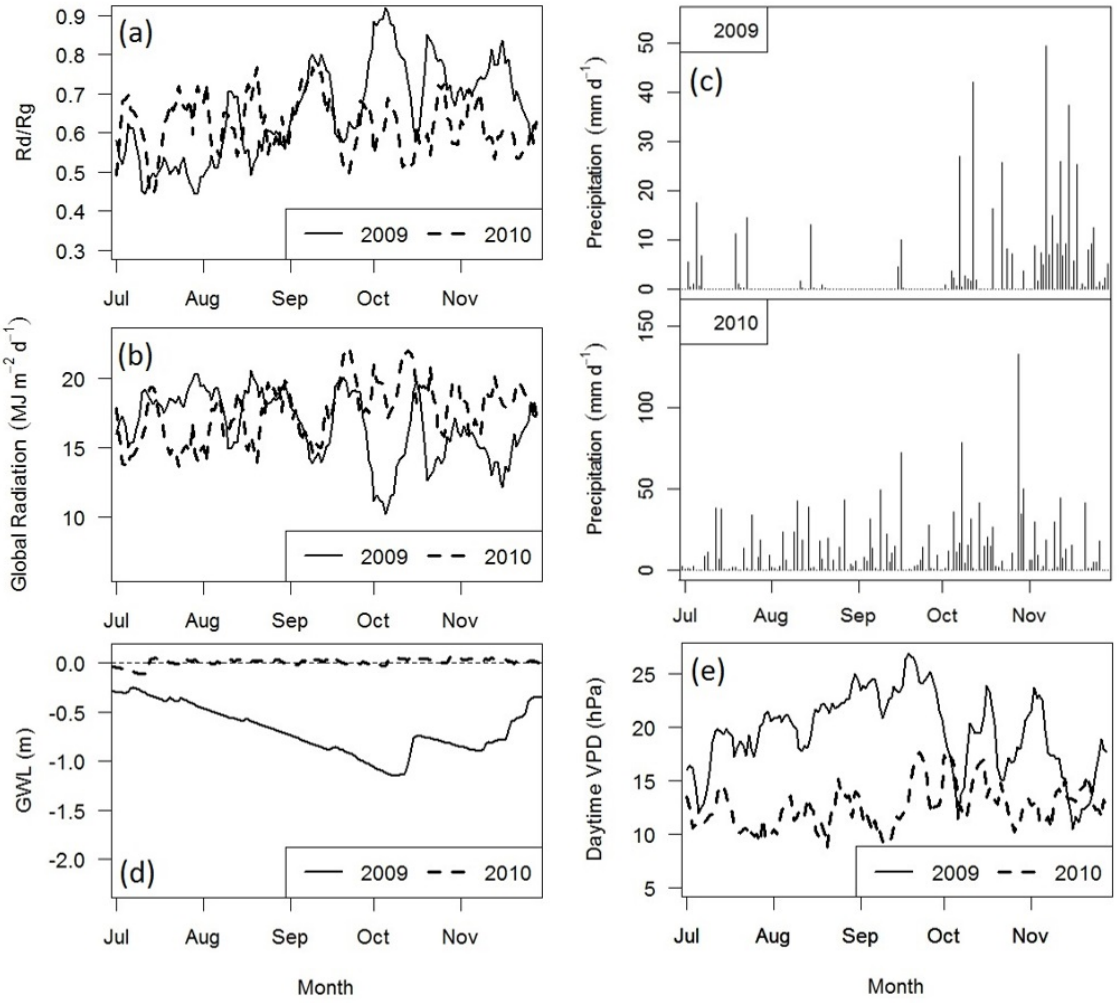

Figure 2.6 Daily variations in the diffuse fraction (R_d/R_g) (a), global solar radiation (R_g) (b), precipitation (c), groundwater level (*GWL*) (d) and daytime vapor pressure deficit (*VPD*) (0900-1500 h) (e) for five months from July to November in 2009 (El Niño year) and 2010 (La Niña year) at DB site. The R_d/R_g, R_g, and *VPD* are shown as 5-day running means.

reflection of solar radiation. Another effect of aerosol on cloud is a reduction of precipitation efficiency and increases the cloud lifetime (Ramanathan *et al.*, 2001). Thus, R_d/R_g remained large above 0.7 for about two months in 2009 (Fig. 2.6). Precipitation in late October in 2009 suggests the formation of persistent cloud particles (ABC; atmospheric brown cloud). The ABC is likely to increase aerosol's hygroscopicity and tends to grow with higher humidity (Fan *et al.*, 2010). After the onset of the rainy season, particle concentration returned to background values by rainfall washout (Heil *et al.*, 2007).

2.5. Conclusions

The diffuse fraction of global solar radiation in tropical peatland was controlled by seasonal variation in precipitation or cloud amount and smoke from biomass burning and peat fires, which are mostly due to human activities. If no fires occur, the diffuse fraction decreases in the dry season as precipitation decreases. In the late dry season, however, fires commonly occur and emit smoke except for in La Niña year with no specific dry period. In particular, during El Niño drought, massive smoke is frequently emitted from large-scale peat fires and densely shades the ground. As a result, the diffuse fraction becomes almost saturated. We parameterized a linear threshold model using field data and found that some parameters differed from those determined in Australia with drier climate. The model is applicable to estimate the diffuse fraction from widely measured global solar radiation for tropical peatland, in which the radiation environment is seriously disturbed.

Chapter 3

Spectral vegetation dynamics and vegetation recovery in a fire-disturbed ex-tropical peat swamp forest

This chapter presents analyses of spectral vegetation dynamics from a meteorological tower (i.e. broadband data), plants phenology, and vegetation recovery in a fire-disturbed ex-tropical peat swamp forest. The analysis fills a gap from the existing studies by taking into account the interaction between PAR (Photosynthetically Active Radiation) and diffuse radiation. For this study, the diffuse fractional estimation shown in Chapter 2 is used. Further analysis of PAR and surface reflectance are performed in this chapter.

In Progress: **Marpaung F, Hirano T 2016: Spectral vegetation dynamics and vegetation recovery in a fire-disturbed ex-tropical peat swamp forest.** (Submitted).

3.1. Introduction

In Southeast Asia, mainly in Indonesia, tropical peatland is widely distributed over 2.07×10^5 km^2 (about 5.21% of global peatland area), and it stores soil up to 57.4 Pg carbon, which accounts for ~ 12% of global peatland area (Page *et al.*, 2011). However, these peatlands have been rapidly devastated by logging, poor land management practices, such as extensive plantation development (Miettinen and Liew, 2010) and enormous drainage in the last decade (Miettinen *et al.*, 2011). The peatlands have also experienced repeatable large-scale fires as a result of land clearing (Murdiyarso and Adiningsih, 2007) and lowered groundwater level (GWL) (Putra and Hayasaka, 2011; Putra *et al.*, 2008) in the late dry season, especially when strong El Niño drought arise (Langner and Siegert, 2009). During these events, smoke from burning biomass and peat fires attenuates solar radiation and increases its diffuse fraction on regional and local scales (Marpaung and Hirano, 2014). The canopy photosynthesis tends to be significantly more light-use efficient under diffuse solar radiation than under direct solar radiation, because diffuse radiation, which is non-directional, penetrates more into the forest canopy (Knohl and Baldocchi, 2008; Oliphant *et al.*, 2011; Roderick *et al.*, 2001). Therefore, the reduction of forest photosynthesis would be depressed by increased diffused radiation and consequently influencing gross primary production (GPP) (Hirano *et al.*, 2012) and forest productivity.

Fire and drought also exert a strong influence on tropical forest metabolism. The fire alters soil properties and reduces plant cover and plant composition, whereas severe drought can increase tree mortality. These conditions along with associated environmental and phenological characteristic give different impact on vegetation regrowth, and ultimately change carbon flux to the atmosphere.

Monitoring forest regrowth and phenology (expressed as leaf area index; LAI) have been widely conducted using surface reflectance that are derived from satellite and meteorological tower data (Baret and Guyot, 1991; Carlson and Ripley, 1997; Huemmrich *et al.*, 1999; Steltzer and Welker, 2006; Wilson and Meyers, 2007). These information are important for ecosystem process because they are able to detect trends, seasonally, and anomalies in forest vegetation dynamic, which are changing due to drought, fires, and climate change.

Despite the extended research carried out about fire effects in tropical peat swamp forest, little information about forest productivity and leaf phenology is available. Most studies have focused on burn severity and its impacts on land cover change using vegetation indices (e.g. normalized difference vegetation index; NDVI) (Hoscilo *et al.*, 2013, 2011; Segah *et al.*, 2010; Tansey *et al.*, 2008), CO_2 exchange (expressed as net ecosystem exchange; NEE), CO_2 emission from the peat, and evapotranspiration (Hirano *et al.*, 2015, 2014, 2012; Sundari *et al.*, 2012). Nevertheless, knowledge about the effects of peat fires on dynamical surface radiation change is quite limited. In addition, satellite-based forest monitoring in this ecosystem is limited because the usability of noise-free satellite images from cloud and aerosols over East and Central Kalimantan provinces, Indonesia, was only 0-1 day per month (Nagai *et al.*, 2014).

In order to identify the trends of vegetation growth and phenology in fire-disturbed tropical peat swamp forest, we evaluate the micrometeorological variables, groundwater level (GWL) from the field, and surface reflectance dataset from the Moderate Resolution Imaging Spectroradiometer (MODIS) and tower, for more than 10 years between 2004 and 2014. First, this study will attempt to investigate the effects of diffuse radiation and peat background in dynamical solar radiation components and

canopy reflectance, and to find a new proportion in the radiation components, especially for the tropical peatland. The parameters of Weiss and Norman (1985), and Wilson and Meyers (2007) models are modified to access visible (VIS) and near infrared (NIR) components and their transmission through the forest canopy in this ecosystem. Second, we used in situ measurements of leaf and tower-based canopy reflectance to examine the seasonal and inter-annual variations of LAI. Finally, we access the change of vegetation conditions through tower-reflectance and peat change after the fires.

3.2. Material and methods

3.2.1. Site description

The field study was conducted between 2004 and 2014 at the DB site (Hirano *et al.*, 2015, 2012) in the upper catchment of the Sebangau River, Central Kalimantan province, Indonesia. The study site (2°20′26.9″S, 114°2′16.4″E) is located in an ex-forest remaining in the northern part of Block C of the Mega Rice Project (MRP): a national project of peatland conversion into rice fields during the late 1990s. The site is about 15 km away from Palangkaraya, the capital of the province, and it was burnt four times during El Niño years in 1997, 2002, 2009, and 2014. The fires changed the cycle of the decline and re-growth of vegetation and also led to loss of surface peat (Hoscilo *et al.*, 2011; Toriyama *et al.*, 2014). Consequently, fern plants have dominated the site. The peat depth is about 4 m with no hummocks on the ground. Ferns (*Stenochlaena*, *Blechnum*, and *Lygodium* spp.) and sedges (*Cyperus, Scleria*, and *Eleocharis* spp.) had grown up to 1 m and covered most of the ground in August 2015 and, burnt coarse woody debris (CWD) from stems, branches, and rootstocks remain on the ground. The

site had been drained by a large canal (25 m wide, 3.5-4.5 m deep), which was excavated in 1996-1997.

Seasonal variation in precipitation was clear. The dry season, which is defined as the number of days with 30-day moving total of precipitation less than 100 mm (Kume *et al.*, 2011), occurs for three to five months from June to October (Hirano *et al.*, 2015; Putra and Hayasaka, 2011) owing to the strong influence of the dry southeast monsoon winds (Aldrian and Dwi Susanto, 2003), whereas the wet season occurs from November to April. Following the seasonal pattern of precipitation, groundwater level (GWL) also showed a clear seasonal variation with a negative peak in the late dry season. El Niño events of 2002, 2006, and 2009 prolonged the dry season and increased the risk of large-scale peat fires by lowering GWL (Hirano *et al.*, 2014; Putra and Hayasaka, 2011). The annual precipitation and annual mean air temperature (mean ± 1 SD) from 2004 to 2014 were 2533 ± 127 mm $year^{-1}$ and 26.4 ± 0.6 °C, respectively, while monthly mean air temperatures were mostly constant within the range of 1 °C.

3.2.2. Field measurements

Meteorological parameters, GWL, and volumetric soil water content (SWC) were measured from April 2004. Radiometers (CNR-1; Kipp & Zonen, Delft, The Netherlands) and quantum sensors (LI-190S; LI-Cor Inc.) measured upward and downward solar radiation, and photosynthetic photon flux densities (PPFD), respectively. Upward PPFD was measured until December 2013. The sensors were mounted on the tip of a 1.5-m-long boom projecting towards the north at the 3.3-m height of a 4-m-tall square tower with a cross-sectional area of 0.4 m × 0.4 m. The tower was extended to 20 m in March 2014 because of tree growth and simultaneously

the sensors were moved to 6.8 m. The field-of-view of the sensors is around 180°, which provides spatial averaging over a circular area with a radius of about 10H (where H is the height of the sensor above the surface). Diffuse radiation was measured with a sunshine sensor (BF3; Delta-T devices, UK) from March 2010 to December 2013, however the data have some gaps due to sensor malfunctions (Marpaung and Hirano, 2014). In addition, air temperature, relative humidity, and precipitation were measured at a height of 1.5 m. Volumetric soil water content (SWC) of the top 30-cm layer was measured with TDR sensors at three points. GWL was measured within 5 m from the tower. These factors were retrieved at intervals of 10 or 30 sec, and their half-hourly means were recorded with a data logger (CR10X; Campbell Scientific Inc., USA). Further information is detailed by Hirano *et al.* (2014).

At the site, four plots with 10 2-m quadrats were set in October 2013. The coverage and height of fern plants were measured every month for each quadrant until September 2014. In September 2014, fern plants were harvested, and an allometry equation to estimate LAI from the monthly data was determined. The site-averaged LAI varied between 1.7 and 2.2 m^2 m^{-2} during the period. After the peat fire of 2009, the fern had grown up about 0.5 m in January 2010 and gradually increased to 0.7 m in October 2013. On the other hand, plant area index (PAI) of fern plants was 2.4 m^2 m^{-2} in June 2006. The plant had grown up to 0.5 m in June 2005 and gradually increased to 0.8-0.9 m in September 2009 (Hirano *et al.*, 2012).

3.2.3. Data analysis

3.2.3.1. Visible and near-infrared components of solar radiation

To apply a plant canopy radiative transfer model and to determine canopy reflectance of the radiation spectrum from a micrometeorological tower, partitioning of the solar spectrum into the direct beam and diffuse components for both visible (PAR) and NIR are needed. This distinction is necessary as the penetration of direct beam and diffuse radiation into the canopy is different. Therefore, we calculated potential PAR (400-700 nm) and NIR (700-2800 nm) components of the total incident solar radiation according to Weiss and Norman (1985). However, the ratio of PAR and NIR depends on solar altitude, and it is strongly affected by atmospheric conditions, especially cloudy conditions in the tropics. Thus, potential values of direct and diffuse PAR components were evaluated in four conditions (i.e. all sky conditions, clear sky conditions, moderate sky conditions, and overcast conditions) using Stigter and Musabilha's approach (1982). We defined a clear sky condition as when the fraction of diffuse radiation (R_d/R_g) was less than 0.2, a moderate sky condition when the R_d/R_g was between 0.2 and 0.9, and an overcast condition when the R_d/R_g was greater than 0.9, during a rainless condition. The R_d/R_g was calculated using measured diffuse solar radiation (R_d, BF3) and global solar radiation (R_g, CNR1) between March 2010 and December 2013, whereas for a long period, R_d/R_g was estimated from a simple linear threshold model (Marpaung and Hirano, 2014; Roderick, 1999) between R_d/R_g and atmospheric transmission/clearness index (R_g/R_o). The R_g/R_o is defined as the ratio of R_g and the extra-terrestrial solar radiation (R_o). R_o (W m^{-2}) was calculated based on solar altitude and time of year (Khan, 2009; Roderick, 1999; Spitters, 1986). In this work, we were not able to evaluate direct and diffuse NIR components because we did not measure the global NIR component. However, at the ground level, the R_g measures three major wavebands: ultraviolet (UV;

305-400 nm), PAR, and NIR but, it is sufficient to lump all PAR and lump all NIR radiation, as the percentage of UV is small or negligible. Hence, the potential values of NIR component in this study were indirectly estimated ($NIR_{est} = R_g - PAR$).

Solar radiation was partitioned into PAR and NIR wavebands using the following equations with η as the ratio of the PAR to solar radiation in a clear sky condition. The potential direct-PAR radiation (R_{DV}) and diffuse-PAR radiation (R_{dV}) on a horizontal surface for the tropics can be approximated by modifying Weiss and Norman's equations (1985) :

$$R_{DV} = \eta \ S_{sc-UV} \ exp\left[-0.185 \left(P/P_o\right) m\right] cos\phi \quad (3.1)$$

$$R_{dV} = R_d/R_g \ (\eta \ S_{sc-UV} - R_{DV}) \ cos\phi \quad (3.2)$$

Moreover, potential direct- (R_{DN}) and diffuse-NIR radiation (R_{dN}) on a horizontal surface for the tropics was calculated from:

$$R_{DN} = \left[(1-\eta) \ S_{sc-UV} \exp\left(-0.06 \left(P/P_o\right) m\right) - w\right] \ cos\phi \quad (3.3)$$

$$R_{dN} = 1 - R_d/R_g \ [(1-\eta) \ S_{sc-UV} - R_{DN} - w] \ cos\phi \quad (3.4)$$

$$\mathrm{m} = (\cos\phi)^{-1} \quad (3.5)$$

$$\omega = 1320 antilog_{10}[-1.1950 + 0.4459 log_{10} m - 0.0345 (log_{10} m)^2] \quad (3.6)$$

where $S_{sc\text{-}UV}$ is a solar constant, excluding the ultraviolet (1320 W m^{-2}), P/P_0 is the ratio of actual to sea level pressure (1013.25 hPa), m is the optical air mass, ϕ is the solar zenith angle, R_d/R_g is the fraction of diffuse radiation, and ω is the water absorption in the near-infrared for 10 mm of precipitable water (adapted from Wang, 1976). Moreover, it is important to note that the quantum sensors measure photon flux density (μmol m^{-2} s^{-1}), whereas the radiometers measure radiation energy density (W m^{-2}). In this study, the conversions were done following Huemmrich *et al.* (1999) using 0.25 for downward PAR, and Ross and Sulev (2000) using 0.2072 for reflected PAR. Estimated

values of total PAR radiation (R_V)_(or total NIR radiation, R_N) were calculated from measured R_g multiplied by the ratio of the PAR ($R_V = R_{DV} + R_{dV}$) (or the ratio of the NIR, $R_N = R_{DN} + R_{dN}$) to the total potential value ($R_T = R_V + R_N$). In addition, data during rain and within an hour after a rain event were excluded to minimize the interference from raindrops on the domes of radiometers.

3.2.3.2. Surface reflectance

Reflectance of the canopy surface was calculated from downward (incident) and upward (reflected) solar radiations and PARs. The sensors were mounted on the north-facing side of the tower above the canopy. Data used for the analysis were collected from April 2004 to December 2014. To eliminate the effect of solar altitude and to avoid the possibility of backward scattering and forward scattering, we used nadir-viewed data; with solar altitude are greater than 60°. The VIS reflectance (R_{VIS}) was calculated by dividing reflected VIS against incoming VIS, whereas the NIR reflectance (R_{NIR}) was calculated by dividing reflected NIR against incident NIR, according to Wilson and Meyers (2007) (see Eqs. 1, 4–6). Incident components of VIS and NIR wavebands during clear skies were calculated as follows:

$$VIS_{in} = \eta \times R_g \tag{3.7}$$

$$NIR_{in} = (1 - \eta) \times R_g \tag{3.8}$$

where VIS_{in} and NIR_{in} are the incidents solar radiation component of VIS and NIR, respectively. In order to estimate the reflected VIS in 2014, we analyzed the linear relationship between R_{NIR} and albedo on a half-hourly basis from April 2004 to December 2013, when solar altitude is greater than 60° in rainless conditions, and substitution of the parameters were done to calculate reflected VIS.

3.2.3.3. Vegetation indices

Spectral vegetation indices (VIs) were calculated both from the tower and from satellite data, which are different in temporal, spatial, and spectral resolutions. By definition, spectral VIs utilize the vegetation absorption of VIS and NIR components. We applied two widely used VIs; NDVI – Normalize Difference Vegetation Index (Tucker, 1979) , and EVI2 – Enhanced Vegetation Index 2 (Jiang *et al.*, 2008), as shown below:

$$\text{NDVI} = \frac{\rho_{NIR}-\rho_{red}}{\rho_{NIR}+\rho_{red}} \tag{3.9}$$

$$\text{EVI2} = 2.5\ \frac{\rho_{NIR}-\rho_{red}}{\rho_{NIR}+2.4\rho_{red}+1} \tag{3.10}$$

where the ρ_{red} and the ρ_{NIR} are the reflectance of red and NIR wavebands domain, respectively. For the tower-based (broadband) data, Huemmrich *et al.* (1999), Jenkins *et al.* (2007), and Wilson and Meyers (2007) proposed replacing the red domain (ρ_{red}) with the VIS (R_{VIS}) and the NIR domain (ρ_{NIR}) with the difference between shortwave solar radiation and VIS (R_{NIR}). However, for satellite-derived VIs, the level one – Terra MODIS gridded of surface reflectance (MOD09A1) between 2004 and 2014 was used. The MODIS VIs were calculated using the surface bidirectional reflectance factor of channel 1 (red: 620 – 670 nm) and channel 2 (NIR: 841 - 876 nm), respectively, for the ρ_{red} and for the ρ_{NIR}. The MODIS data were the global time series data recorded as an 8-day composite in 500-m spatial resolution. We retrieved MODIS data from the EOS data gateway (ORNL DAAC, 2015) and subset into a 2.5 km x 2.5 km in size. Due to a high-structured mosaic of vegetation cover, we extracted an area of 1.5 km x 1.5 km, which was the northeast of the tower where re-growing vegetation was dominant. We only used the data, if the quality control variable MODLAND was 0000 (highest quality) related to surface reflectance, and the state flags were 00 or 01 (climatology, or a low aerosol quantity) related to cloud conditions. Consequently, the data in 2014 were

all excluded because of low data quality. Detailed descriptions of the MODIS data are reported in the literature (e.g., http://daac.ornl.gov/MODIS/modis.html).

3.2.3.4. Leaf area index

We computed VIS transmittance using a radiative transfer model to derive leaf area index (LAI) values based on the inversion of the Beer-Lambert law exponential light extinction through plant canopies, as follow:

$$I/I_o = exp(-k \times LAI) \tag{3.11}$$

where the I is the transmitted radiation below canopy, I_o is the incident radiation above the canopy, LAI is the projected leaf area index, and k is the leaf extinction coefficient for incident irradiance. The k was set as an ellipsoidal distribution function of solar zenith angle (ϕ) for a random distribution of spherical leaves in the canopy (Campbell, 1986) (Eq. 3.12), with parameter x as the ratio of average projected areas of canopy elements on horizontal and vertical surfaces (≅1).

$$k_{be}(\phi) = \frac{\sqrt{x^2 + tan^2\phi}}{x + 1.774(x+1.182)^{-0.733}} \tag{3.12}$$

The I_o was measured from the tower, whereas the I was estimated from the light intercepted by canopies. The light interception was calculated from the transmitted and the reflected radiations by the fern and the soil because ferns with sparse canopies dominated the site, and the proportional distribution of the leaves within its canopy structure is a function of fern height. Moreover, due to the non-homogeneity of incident shortwave irradiance, it is usually segmented into portions that are treated separately (Goudriaan, 1977; Ross, 1981), i.e. (1) wavelength bands: VIS versus NIR, and (2) angular distribution: single-angular (direct) radiation versus multi-angular (diffuse)

radiation. However, we only took into account the distinction between direct and diffuse VIS wavelengths.

We estimated the direct and diffuse radiation transferee in sparse canopies with soil reflectance effects, according to Monteith and Unsworth (2013), Campbell *et al.* (1986, 1990); Campbell and Norman (1998), and Spitters (1986). The reflection, transmission, and absorption of diffuse VIS light by the canopies and the soil were calculated using the following equations.

$$\rho_{d,cpy} = \frac{\rho^*_{d,cpy} + \left[\frac{\rho^*_{d,cpy} - \rho_s}{\rho^*_{d,cpy}\rho_s - 1}\right] exp\left(-2\sqrt{\alpha}k_d L_t\right)}{1 + \rho^*_{d,cpy}\left[\frac{\rho^*_{d,cpy} - \rho_s}{\rho^*_{d,cpy}\rho_s - 1}\right] exp\left(-2\sqrt{\alpha}k_d L_t\right)} \tag{3.13}$$

$$\rho^*_{d,cpy} = \frac{2k_d}{k_d + 1}\rho^H_{cpy} \tag{3.14}$$

$$\rho^H_{cpy} = \left(\frac{1-(1-\alpha)^{1/2}}{1+(1-\alpha)^{1/2}}\right)\left(\frac{2}{1+1.6\sin\phi}\right) \tag{3.15}$$

$$\tau_{d,cpy} = \frac{\left[\left(\rho^*_{d,cpy}\right)^2 - 1\right] exp\left(-2\sqrt{\alpha}k_d L_t\right)}{\left(\rho^*_{d,cpy}\rho_s - 1\right) + \rho^*_{d,cpy}\left(\rho^*_{d,cpy} - \rho_s\right) exp\left(-2\sqrt{\alpha}k_d L_t\right)} \tag{3.16}$$

$$\alpha_{d,cpy} = 1 - \rho_{d,cpy} - \tau_{d,cpy}(1 - \rho_s) \tag{3.17}$$

$$f_d = 1 - \tau_d \tag{3.18}$$

where the $\rho_{d,cpy}$ and the$\rho^*_{d,cpy}$ are the diffuse reflection coefficient for sparse canopies and a closed canopies, respectively, the ρ^H_{cpy} is the canopy hemispherical reflection coefficient of a green light in closed canopies, the $\tau_{d,cpy}$ is the diffuse flux density of VIS light under the sparse canopy, the $\alpha_{d,cpy}$ is the diffuse flux density of the VIS light absorbed by the canopy, the f_d is the diffuse radiation intercepted by the canopy, τ_d is the fraction of VIS light transmitted by a canopy, the α is the leaf absorptivity (≅ 0.819), the ρ_s is the soil reflectivity as the averaged from dry and wet bare ground (≅ 0.08, adopted from Dickinson, 1983), and the L_t is the fern height (m). The sparse canopies were determined from the value of LAI which ranges below a rather imprecise threshold

of 2 ~ 4 m^2 m^{-2} (adopted from Carlson and Ripley, 1997). For the direct VIS forms of Eqs. 3.13 - 3.18, k_d (≅ 0.7 for LAI < 3) in diffuse radiance was replaced by $k_{be}(\phi)$ in direct radiance. Then, we calculated LAI using Norman's equation (Norman, 1979):

$$\text{LAI} = \frac{\left[\left(1-\frac{1}{k_d}\right)f_d - 1\right] ln\tau_d}{A(1-0.47f_d)} \tag{3.19}$$

where $\text{A} = 0.283 + 0.785\alpha_{d,cpy} - 0.159{\alpha_{d,cpy}}^2$.

We have no reason to suspect that leaf exposure, clumping or tip angle change seasonally, though we cannot exclude this possibility. We minimized the solar zenith angle effect by considering data observations when solar zenith angle was less than 30°. We set assumptions in using the model to determine LAI, viz., (1) leaf exposure, clumping, and tip angle remain constant, (2) solar angle is controlled for, (3) the proportion of transmittance below canopy was large due to sparse canopies, and (4) plant height from 2005 to 2014 was interpolated based on observation data. The VIS fractional interception of direct and diffuse radiation was averaged to determine daily values of LAI. We cross-validated the values with the semi-direct measured LAIs. All statistical analysis including Pearson correlation and linear regression were conducted using Rstudio (version 0.99.486).

3.3. Results

3.3.1. Partitioning solar radiation into wavebands

To determinate the fraction of VIS radiation in the tropics that is strongly affected by sky conditions, we evaluated the ratio (η) of PAR to total solar radiation in all sky conditions, clear sky conditions, moderate conditions, and overcast conditions (Table 3.1). In the diurnal cycle during all sky conditions, the ratio increased in response to the R_d/R_g and solar zenith angle (ϕ) with its minimum of 0.54 around noon

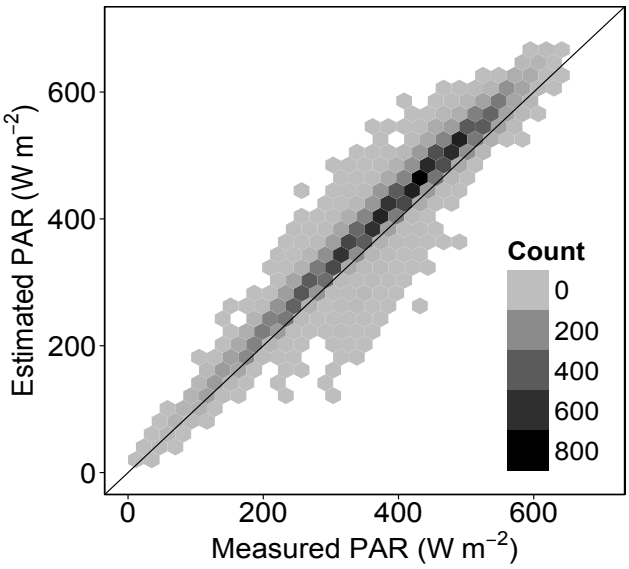

Figure 3.1 A comparison of estimated visible waveband (PAR) with measured photosynthetically active radiation (PAR) on a half-hourly basis for 11 years of 2004 - 2014. Data during rainless condition around midday (0930 – 1330 h, solar zenith angle ≤ 30°) were only used. The slope of the estimation is 1.076.

($\phi < 10°$), and the maximum of 0.61 around sunrise and sunset ($\phi > 80°$). However, the η was constant with 0.55 ± 0.04 (mean ± 1 SD) around midday ($\phi \leq 30°$) The η also performed in the same way during moderate sky and overcast conditions, with a higher value occurred during early morning and late afternoon ($\phi > 70°$) because of the effects of sunrise and sunset. In contrast, the η was almost constant during clear sky conditions. In addition, during overcast conditions ($\phi < 70°$), the η (mean ± 1SD) was higher in the dry season (0.60 ± 0.21) than in the wet season (0.56 ± 0.05) due to dense smoke emitted through biomass burning and peat fires in the latter half of the dry season, particularly during El Niño years (Marpaung and Hirano, 2014).

Table 3.1 The ratio of PAR to solar radiation on a half-hourly basis during rainless conditions*.

ϕ (°)	All conditions[B]			Clear sky condition[C] ($R_d/R_g < 0.2$)			Moderate condition[C] ($0.2 \le R_d/R_g \le 0.9$)			Overcast condition[A] ($R_d/R_g > 0.9$)		
	η	R_d/R_g	ϕ (°)	η	R_d/R_g	ϕ (°)	η	R_d/R_g	ϕ (°)	η	R_d/R_g	ϕ (°)
0-10	0.54^{k}	0.56	6.64	$0.54^{j,k}$	0.18	6.77	0.54^{k}	0.52	6.62	$0.56^{i,j,k}$	0.95	6.82
10-20	0.55^{k}	0.56	15.81	0.55^{k}	0.18	15.77	0.54^{k}	0.53	15.80	$0.56^{i,j,k}$	0.95	15.91
20-30	$0.55^{j,k}$	0.56	25.05	0.54^{k}	0.18	25.25	0.55^{k}	0.52	25.04	$0.56^{h,i,j}$	0.95	25.17
30-40	$0.55^{i,j,k}$	0.57	34.83	0.55^{k}	0.18	33.87	$0.55^{i,j,k}$	0.52	34.80	$0.56^{g,h,i}$	0.95	35.16
40-50	$0.56^{i,j}$	0.60	44.83	$0.55^{i,j,k}$	0.18	44.49	$0.56^{i,j,k}$	0.54	44.79	$0.57^{f,g,h}$	0.95	45.03
50-60	$0.57^{g,h}$	0.66	55.15	0.54^{k}	0.18	54.90	$0.56^{h,i}$	0.58	55.08	$0.59^{c,d}$	0.95	55.44
60-70	$0.58^{e,f}$	0.72	65.12	0.54^{k}	0.17	64.99	$0.58^{f,g}$	0.63	65.00	$0.58^{d,e,f}$	0.95	65.38
70-80	$0.58^{d,e}$	0.80	74.80	$0.55^{i,j,k}$	0.16	72.56	$0.58^{d,e,f}$	0.68	74.49	0.59^{d}	0.95	75.17
80-90	$0.61^{a,b}$	0.87	83.84	NA	NA	NA	$0.60^{b,c}$	0.75	83.94	0.62^{a}	0.95	83.78
Mean	0.57	0.66		0.55	0.18		0.56	0.57		0.59	0.95	
±1SD	±0.10	±0.12		±0.03	±0.01		±0.10	±0.19		±0.20	±0.02	

η ratio of PAR to solar radiation; R_d/R_g fraction of diffuse radiation; ϕ solar zenith angle

* The *P*-value of ANOVA < 0.001

Different uppercase letter denote significant difference among sky conditions at significant level of 0.001 according to Tukey's HSD

Different lowercase letter in each column denote significant difference among solar zenith angle at significant level of 0.05 according to Tukey's HSD

Overall, the ratio in overcast conditions was higher than other sky conditions. The ratio was not different during a clear sky and a moderate sky conditions. The values (mean ± 1 SD) were 0.57 ± 0.10, 0.55 ± 0.03, 0.56 ± 0.10, and 0.59 ± 0.20, respectively, for all sky conditions, clear sky condition, moderate sky conditions, and overcast condition (Table 3.1). In addition, the η of 0.55 was also feasible for daily analysis because of the higher ϕ of 70° were excluded in data analysis in order to eliminate the effects of sunrise and sunset. Furthermore in daily analysis, we excluded all data during smokes and fires.

Owing to the relative constant value of η during all-, clear-, and moderate-sky conditions in diurnal cycle, we set the η to be 0.55 (expressed as alternative model) to estimate VIS. Simple linear correlation between the estimated PAR and the measured PAR for half-hourly midday data showed a significant relationship with r^2 of 0.99 and

Table 3.2 The support for the estimative models and its comparison.

Model	Sky Conditions	AIC_C	ΔAIC_C	Slope	RMSE	R^2
Default	Clear	691	0	1.12	21.07	1.00
	Moderate	100030	3126	1.13	27.11	0.99
	Overcast	21006	0	1.16	16.50	0.97
	All	100030	3126	1.13	27.11	0.99
Alternative	Clear	701	10	0.94	22.48	1.00
	Moderate	**96904**	0	0.93	23.86	0.99
	Overcast	21246	240	0.87	16.97	0.96
	All	**96904**	0	0.93	23.86	0.99

Estimative models were characterized by η (Eq. 3.1 - 3.4, 3.7), where default model used η of 0.45, and alternative model used the η of 0.55 for the tropical peatland. η is the ratio of PAR to solar radiation, AIC_C is the corrected Akaike Information Criterion, RMSE is the is the root-mean-square of the difference estimated VIS and measured VIS, Slope is based on a linear fit with zero intercept, and R^2 is the determination coefficient of the regression line. The model with the strongest support in data is shown in boldface type. For the comparison, data during rainless condition around midday are used.

RMSE of 23.86 W m^{-2} (Fig. 3.1). This alternative model also showed the most support model for sky conditions over tropical peatland. The value of evidence in support of this model was high during moderate- and all-sky conditions, and the value of evidence supporting the alternative model during clear sky conditions was relatively same with the default model. There was a little support for the model in overcast conditions. (Table 3.2).

3.3.2. Seasonal variation of surface reflectance and environmental factors

Seasonal variations in surface reflectance and environmental factors are shown in the time sequence of monthly values in Fig. 3.2. According to sea surface temperature (SST) anomaly in Niño 3.4 Region (NOAA, http://www.cpc.ncep.noaa.gov/data/ indices/ersst4.nino.mth.81-10.ascii) (Fig. 3.2a), El Niño events occurred in the period of 2004 - 2005, 2006 - 2007 and 2009 - 2010, and La Niña events occurred in the periods of 2007 - 2008, 2010 - 2011 and 2011 - 2012. Precipitation varied seasonally with a shift owing to El Niño and La Niña events (Fig. 3.2b). Groundwater level (GWL) (Fig. 3.2c) and volumetric soil water content (SWC) (Fig. 3.2d) at a depth of 5 cm varied in accordance with precipitation variation, whereas water vapor pressure deficit (VPD) increased as precipitation decreased (Fig. 3.2e). After the peat fire in 2009, SWC in the wet seasons decreased, because soil bulk density was increased by peat burning. Albedo showed a clear seasonal variation with a peak in the dry seasons and a trough in the wet seasons (Fig. 3.2g). A lower albedo in 2004 - 2005 was due to the less-vegetated ground surface that was studded with open water (Hirano *et al.*, 2015), whereas the large increased albedo in the dry seasons of 2006 and 2009 was caused by a massive amount of smoke emitted from large-scale fires that led to low global solar radiation (Fig. 3.2f). Moreover, these massive smoke emitted from

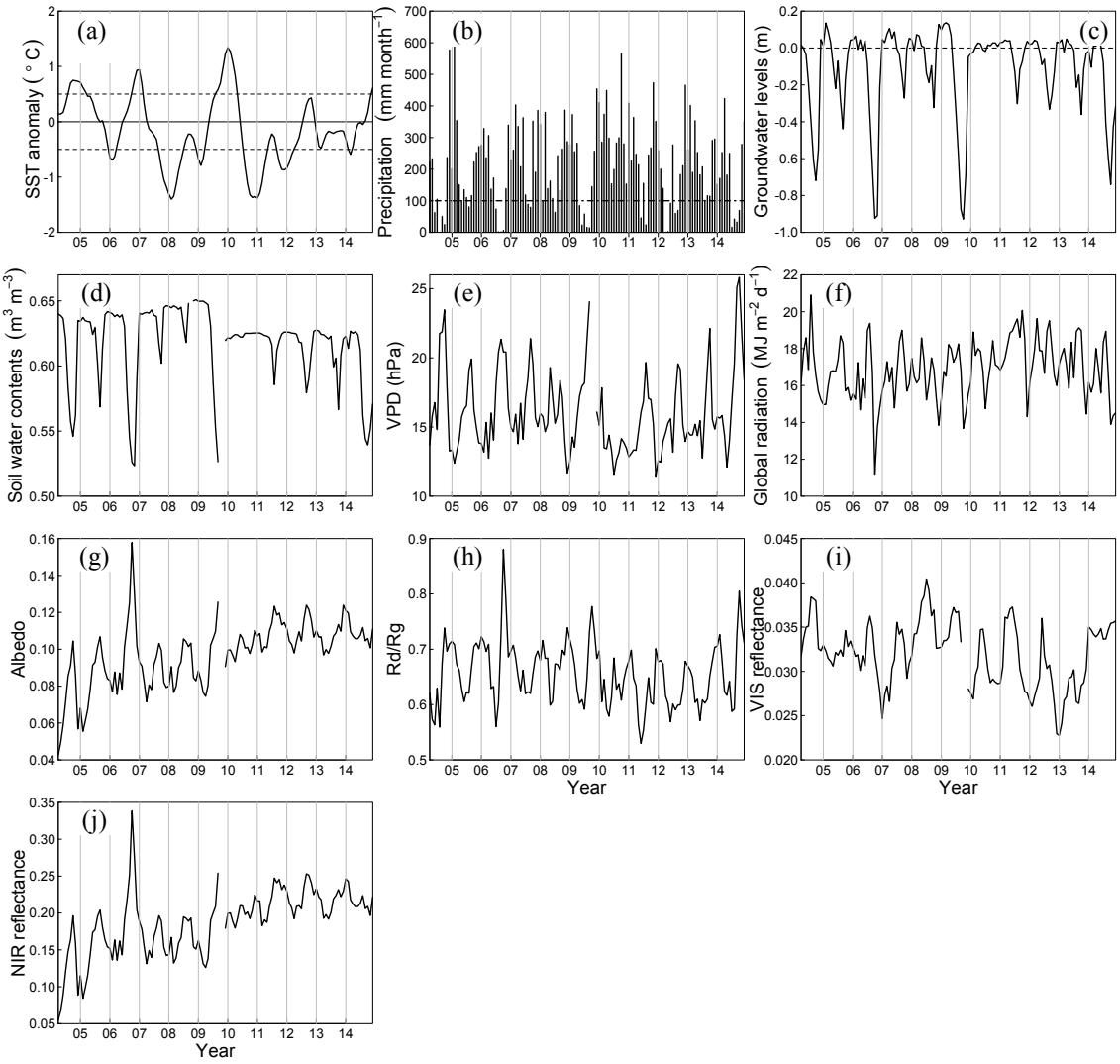

Figure 3.2 Time series of monthly values of sea surface temperature (SST) anomaly (a), precipitation (b), groundwater level (c), volumetric soil water content (d), daytime (900-1500 h) vapor pressure deficit (VPD) (e), global solar radiation (f), albedo (g), diffuse fraction (R_d/R_g) (h), visible (VIS) reflectance (i), and near-infrared (NIR) reflectance (j), from April 2004 to December 2014. El Niño and La Niña events are defined as 5 consecutive months of running 3-month mean at or above the +0.5 anomaly, and at or below the -0.5°C anomaly, respectively.

peat burning and forest fires in 2006 and 2009, which have a large particle size (Ikegami *et al.*, 2001), increased forward scattering in the NIR wavelength, and hence it increased NIR reflectance. Notwithstanding the difference from smoke and soil background, the NIR reflectance closely followed the albedo reaching a maximum value of about 0.34 with the highest albedo of about 0.16 (Fig. 3.2j), whereas the VIS reflectance distantly

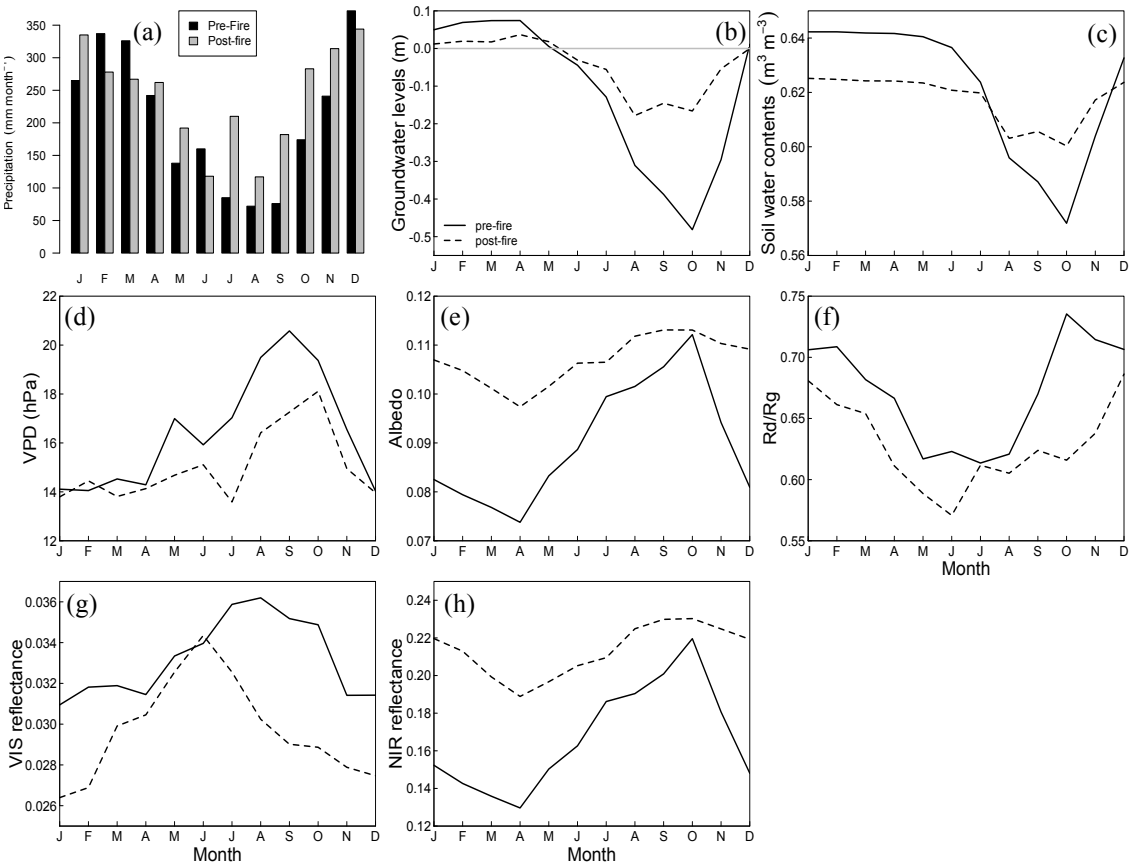

Figure 3.3 Mean seasonal variations in monthly values of precipitation (a), groundwater level (b), volumetric soil water content (c), daytime (900-1500 h) water vapor deficit (VPD) (d), albedo (e), diffuse fraction (R_d/R_g) (f), visible (VIS) reflectance (g), and near-infrared (NIR) reflectance (h) before the peat fire of 2009 (August 2004 – August 2009) (solid line), and after the peat fire of 2009 (December 2009 – December 2014) (dashed line).

followed the albedo (Fig. 3.2i). VIS reflectance fluctuated in accordance with diffuse solar radiation fraction (R_d/R_g) (Fig. 3.2h).

To clearly investigate seasonal variation of surface reflectance in relation to environmental factors, monthly values were averaged for two periods; before the fire in September 2009 (August 2004 - August 2009) and after the fire (December 2009 – December 2014) (Fig. 3.3). On average, in the pre-fire period, the dry season was prolonged until November in 2004, 2006 and 2009 due to El Niño events, whereas the dry season did not clearly occur in 2010 because of a La Niña event (Figs. 3.2a, 3.2b, and 3.2c). Following the precipitation variation (Fig. 3.3a), GWL and SWC were lower

before the fire than after the fire (Fig. 3.3b and 3c). The lowest GWL occurred in October (-0.48 m) before the fire and in July (-0.18 m) after the fire. Seasonal variation in SWC was in parallel with GWL. In addition, VPD was higher before the fire. Albedo increased after the fire and showed a similar seasonal variation with a peak in October both before and after the fire, whereas its annual range was smaller after the fire (Fig. 3.3e). Similarly, NIR reflectance reached a peak in October and a trough in April for both periods (Fig. 3.3h). In contrast, VIS reflectance varied seasonally in reverse parallel with R_d/R_g variation (Figs 3.3f and 3.3g). VIS reflectance sharply increased from the late wet season to the early dry season. During the dry season in the pre-fire period, VIS reflectance remained high with a sharp increase in R_d/R_g.

3.3.3. Environmental response of vegetation indices

The relationship of the VIs with GWL or SWC was analyzed using 8-day mean data around midday ($\phi \leq 30°$) in rainless conditions (Fig. 3.4). In unflooded conditions (GWL <0 m or SWC < 0.62 m^3 m^{-3}), broadband NDVI showed insignificant relationship with GWL or SWC. However, NDVI showed significant negative linearity with GWL (r^2 = 0.58, p < 0.001) or SWC (r^2 = 0.37, p < 0.001) during flooded conditions. In similar to NDVI, EVI2 significantly decreased as GWL increased and SCW increased (GWL: r^2 = 0.43, p < 0.001, SWC: r^2 = 0.59, p < 0.001) in flooded conditions. These negative relationships indicate that the broadband NDVI and EVI2 tended to decrease as GWL or SWC increased above 0 m or 0.62 m^3 m^{-3}. Of particular interest is the dominant open area with a less vegetation on the ground during 2004 caused a low value in NDVI (± 0.5) and EVI2 (± 0.2) in the curve (Fig. 3.4).

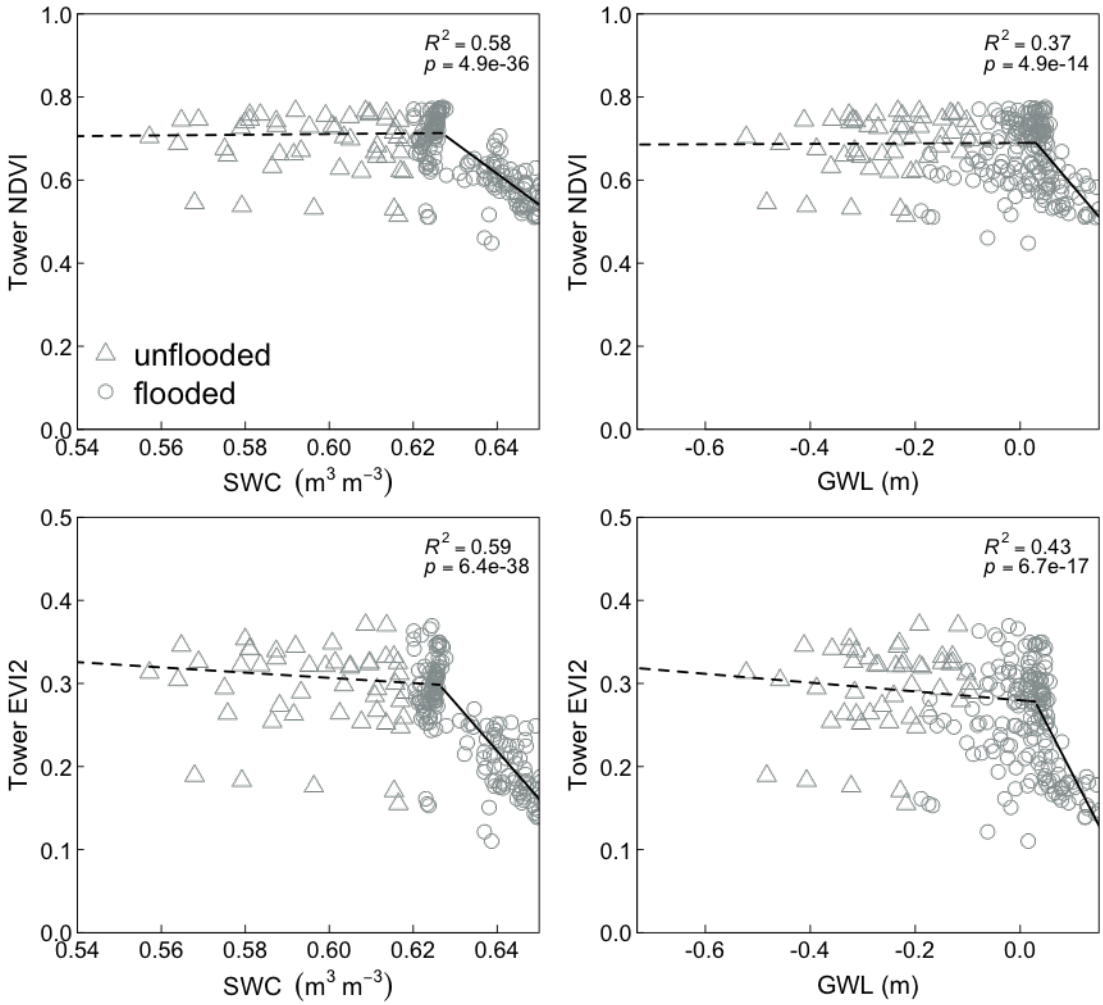

Figure 3.4 Relationship between tower-based NDVI or EVI2 and groundwater level (GWL) or volumetric soil water content (SWC) on an 8-day-mean basis from 2004 to 2014. Different lines were fitted to data sets at GWLs of 0 m and SWC at about 0.62 m^3 m^{-3}. For the purpose of soil moisture conditions, data points are split into 'flooded' (circle), and 'unflooded' (triangle) conditions, using GWL and SWC of greater than 0 m, or 0.62 m^3 m^{-3}, and less than 0 m or 0.62 m^3 m^{-3}, respectively. Significant solid lines were fitted to datasets at SWCs greater than 0.62 m^3 m^{-3} (r^2 > 0.58) or at GWLs greater than 0 m (r^2 > 0.37). Data during fires and smokes events were excluded.

3.3.4. Variation in vegetation indices

Variations in NDVI and EVI2 for 10 years are shown in Fig. 3.5 along with R_d/R_g. Broadband NDVI varied seasonally with a high magnitude in the pre-fire period. It reached a base in April and a peak in October for both periods. On the other hand, MODIS NDVI showed low seasonality throughout the years. It varied seasonally in

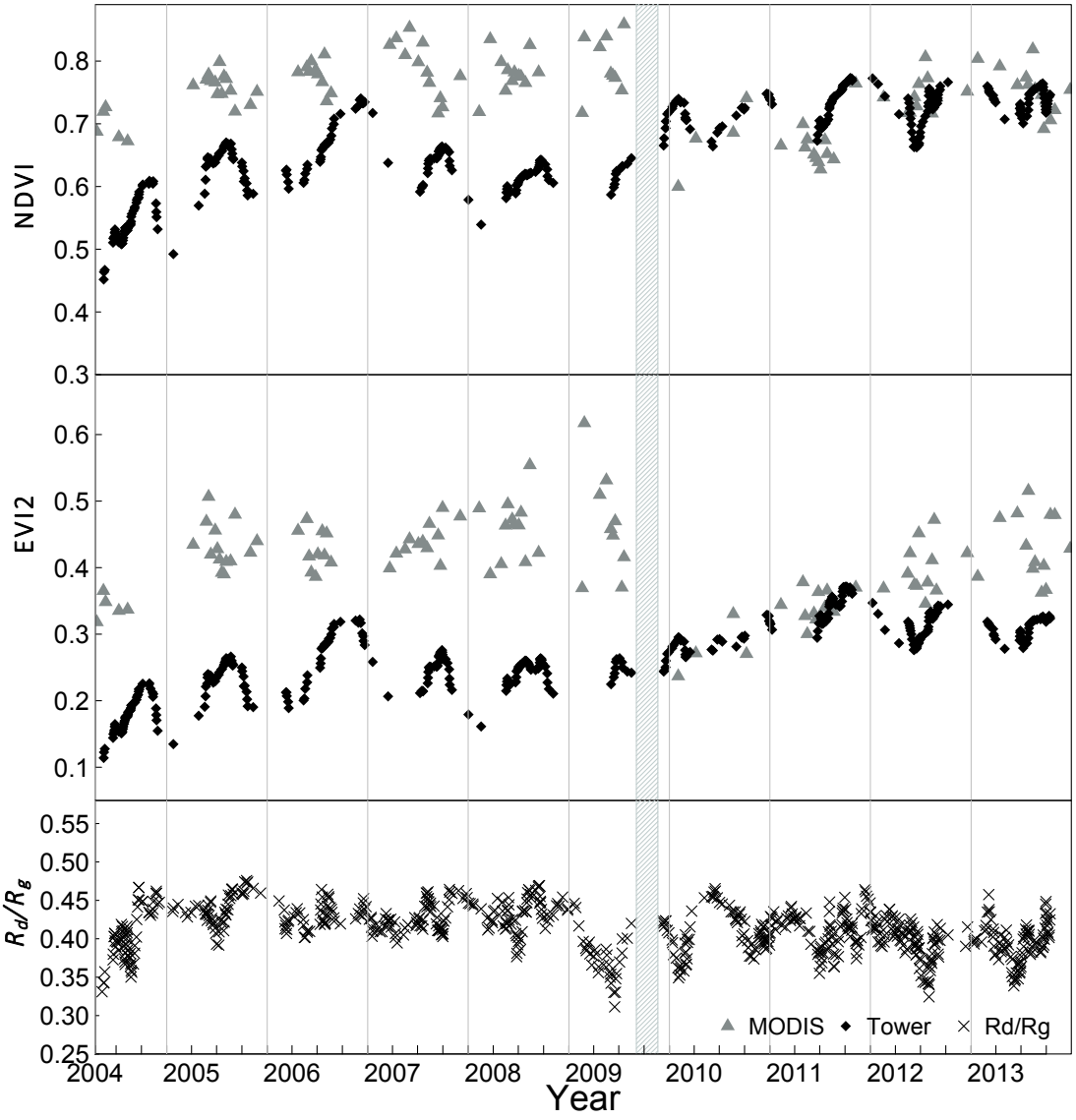

Figure 3.5 Variation in 8-day averaged broadband (tower-based) NDVI, (tower-based) broadband EVI2, MODIS NDVI, MODIS EVI2, and diffuse radiation (R_d/R_g) from April 2004 to December 2013. Data during fires, smokes events, and flooded conditions were excluded. During the gray period, the site was burnt.

parallel with broadband NDVI for both periods and showed a negative linearity with 8-day averages VIS reflectance (figure not shown, $r^2 = 0.21$, $p < 0.05$) after the fire.

The annual average of NDVI in the pre-fire period was 0.77, and 0.63, respectively for MODIS and broadband NDVI. After the peat fire of 2002, the NDVI increased and reached its maximum of 0.85 in the latter of 2009, and 0.74 in the latter of 2006, respectively, for MODIS and broadband NDVI. Low broadband NDVI in April

2004 and early 2005 were due to less-vegetated ground that was studded with open water (Hirano *et al.*, 2015). Unlike NDVI before the fire, in the post-fire period, the broadband was similar to those of MODIS with an annual average of 0.71 and 0.72, respectively, for MODIS and broadband NDVI. In general, the NDVI values from MODIS exceeded those from the broadband for both periods; with the broadband NDVI and MODIS NDVI, values were much closer in the post-fire period (Table 3.3).

The difference in surface greenness was much pronounced for EVI2 than NDVI (Fig. 3.5, Table 3.3). The slopes between broadband and MODIS EVI2 were 0.55 and 0.73 with RMSE values of 0.004 and 0.04, respectively, for the pre-fire and the post-fire periods. The surface greenness, as expressed broadband EVI2, was lower than broadband NDVI at the burned site in the latter of 2009 and followed similar seasonal

Table 3.3. Comparison* between vegetation indices derived from MODIS and radiation tower (broadband) data in 8-day averages from 2004 to 2013 at DB site.

Vegetation Indices Comparison	Season	N	Slope	R^2	RMSE
Tower vs. MODIS NDVI	Pre-Fire	15	0.81	0.99	0.049
	Post-Fire	12	0.98	0.99	0.064
Tower vs. MODIS EVI2	Pre-Fire	15	0.55	0.98	0.004
	Post-Fire	12	0.73	0.96	0.042

* N is the number of observations, RMSE is the root-mean-square of the difference between tower and MODIS values, Slope is based on linear fit with zero intercept, and R^2 is the determination coefficient of the regression line. All the regression is significant at the 95% confidence interval.

patterns observed for broadband NDVI and albedo. Contrary with MODIS NDVI, correlation between MODIS EVI2 and the 8-day averages VIS reflectance was not found. During the pre-fire period, the inter-annual variation of broadband and MODIS EVI2 was small with the annual average of 0.24, and 0.43, respectively. The higher MODIS EVI2 observed in 2009 could be attributed to atmospherically induced variations associated with smoke. The broadband EVI2 reached its maximum of 0.32 in

November 2006, whereas MODIS EVI2 reached its maximum of 0.61 in early 2009. The EVI2 sharply dropped in the latter of 2009. Similar to EVI2 during the pre-fire period, the inter-annual variation of broadband and MODIS EVI2 was small with the annual average of 0.30 and 0.36, respectively during the post-fire period. Moreover, the EVI2 reached its maximum value of 0.37 in the latter of 2011, and 0.43 in July 2013, respectively for broadband and MODIS.

3.3.5. Variation in leaf area index

A continuous amount of VIS intercepted by the fern canopies that was measured from the tower was used to calculate seasonal variations of LAI. This approach is appropriate for determining the relative seasonal changes in LAI (Bréda, 2003; Wang *et al.*, 2004b). In addition, the transmitted VIS wavelength band ($\tau_{b,cpy}(\phi)$ or $\tau_{d,cpy}$) is a reasonable approximation to LAI (Campbell and Norman, 1998), and relatively insensitive to changes in the spectral reflectance of leaves.

Generally, seasonal variations of LAI, which is calculated from the VIS interception of direct or diffuse radiation were almost the same, though the LAI of VIS direct interception was higher than diffuse interception. The direct-estimated LAI was 1.4 higher than diffuse-estimated LAI (Fig. 3.6). The seasonal variations also did not differ across the periods (Fig. 3.7). During the pre-fire period, the LAI reached a minimum in March-April and a maximum in September. However, in the latter of 2006 and 2009, dense smoke emitted from the peat fires stepped up surface reflectance, and consequently resulted in an overestimated LAI. Similar with LAI during the pre-fire period, LAI varied seasonally with a peak in August during post-fire period. However,

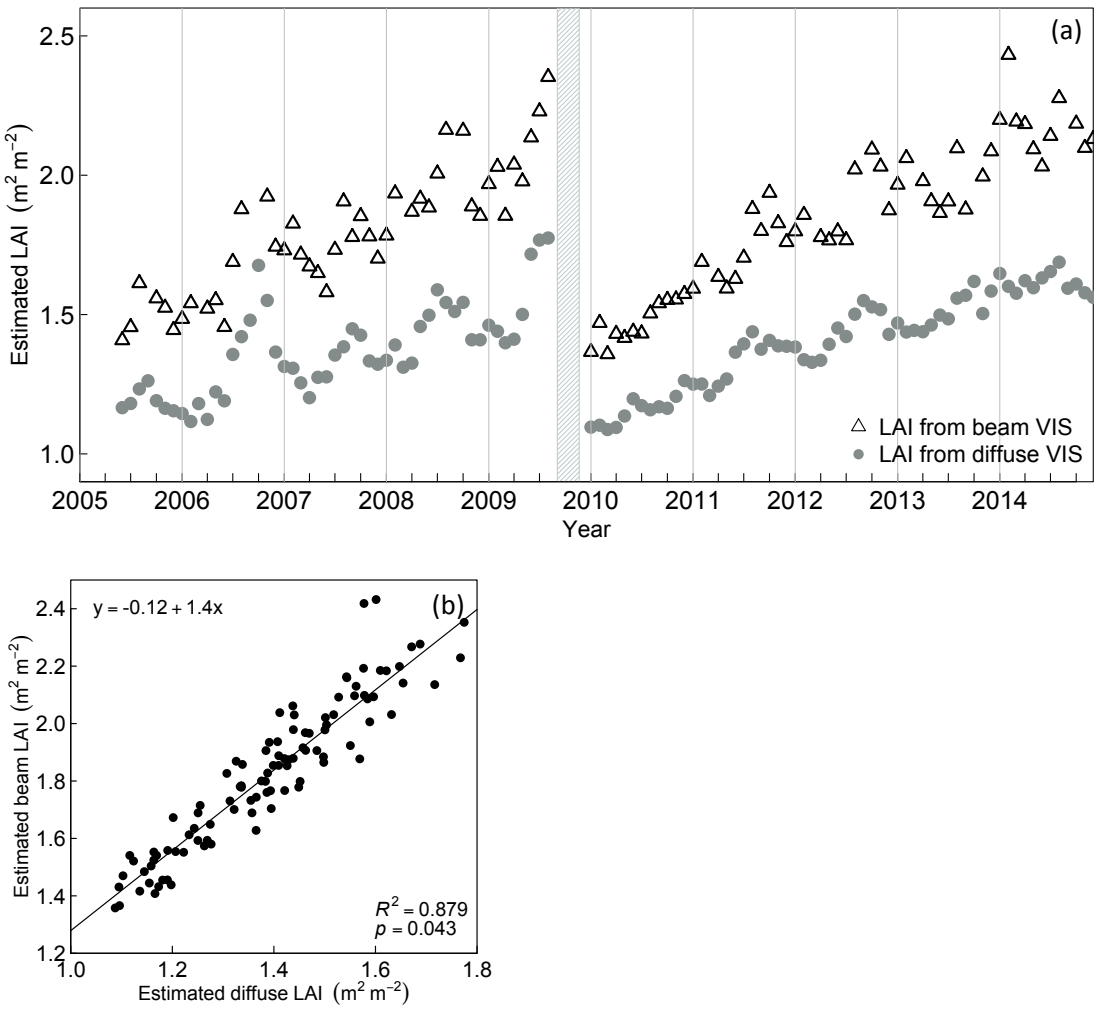

Figure 3.6 Analysis of the relationship between beam- and diffuse-transmitted VIS wavebands to estimate LAI. **a.** The time sequence of monthly average of estimated LAI, and **b.** Comparison between monthly averages direct (beam) LAI and diffuse VIS LAI.

seasonal variation of semi-direct LAI, which had been done for one year, was not clear, though it slightly decreased through the early wet season of 2013, continued to increase from January 2014 to August 2014, and then slightly decreased in September 2014. In addition, the site was burnt in September 2014, although the fire damage was not so large.

A comparison between monthly average of estimated LAI and semi-direct LAI is shown in Figure 3.8. In spite of the fact that we were only able to measure monthly LAI for the ferns, which is dominant vegetation in DB site; the scatter plot showed a good statistical agreement ($r^2 = 0.99$, $p < 0.001$, $N = 12$). Slope of the straight lines with

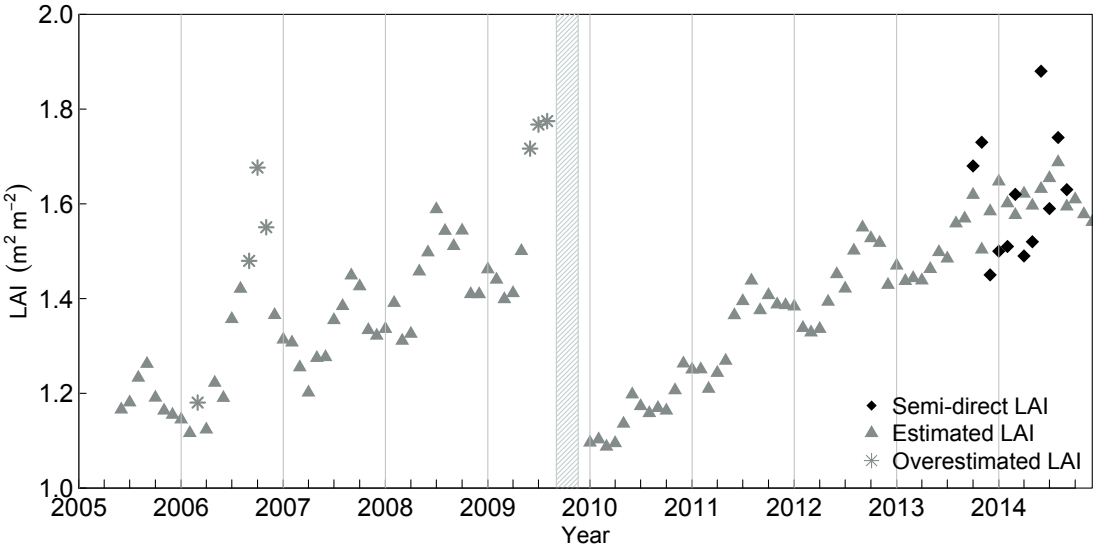

Figure 3.7 Time sequence of monthly average of estimated and semi-direct LAI from June 2015 to December 2014. The gray area shows a peat fire occurred in DB site. Semi-direct LAI was measured for 1 year from October 2013 to September 2014.

zero intercept between the estimated and semi-direct LAI was 0.99 with RMSE values of 0.13 m^2 m^{-2}. The annual LAI (mean ± 1 SD) from October 2013 to September 2014 was 1.62 ± 0.44 m^2 m^{-2} and 1.61 ± 0.07 m^2 m^{-2}, respectively, for semi-direct LAI and estimated LAI. In addition, the sensitivity of LAI retrieval to the variation of plant

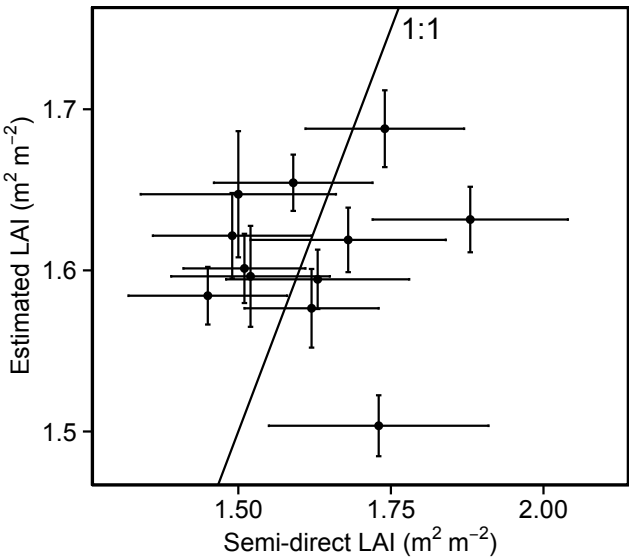

Figure 3.8. Comparison between monthly averages estimated LAI and semi-direct LAI in DB site for 1 year from October 2013 to September 2014. Vertical bars and horizontal bars denote one standard error of estimated LAI and semi-direct LAI, respectively.

height from the model was evaluated. The LAI model is sensitive to plant height (Fig. 3.9). It raised double from 0.9 m^2 m^{-2} to 1.8 m^2 m^{-2} as the plant height increased from 0.2 m to 1.0 m, independently of date (Fig. 3.9). However, the LAI is less sensitive to plant height in July 2014 ($p > 0.05$, Fig. 3.9c) owing to an increasing vegetation cover in 2014.

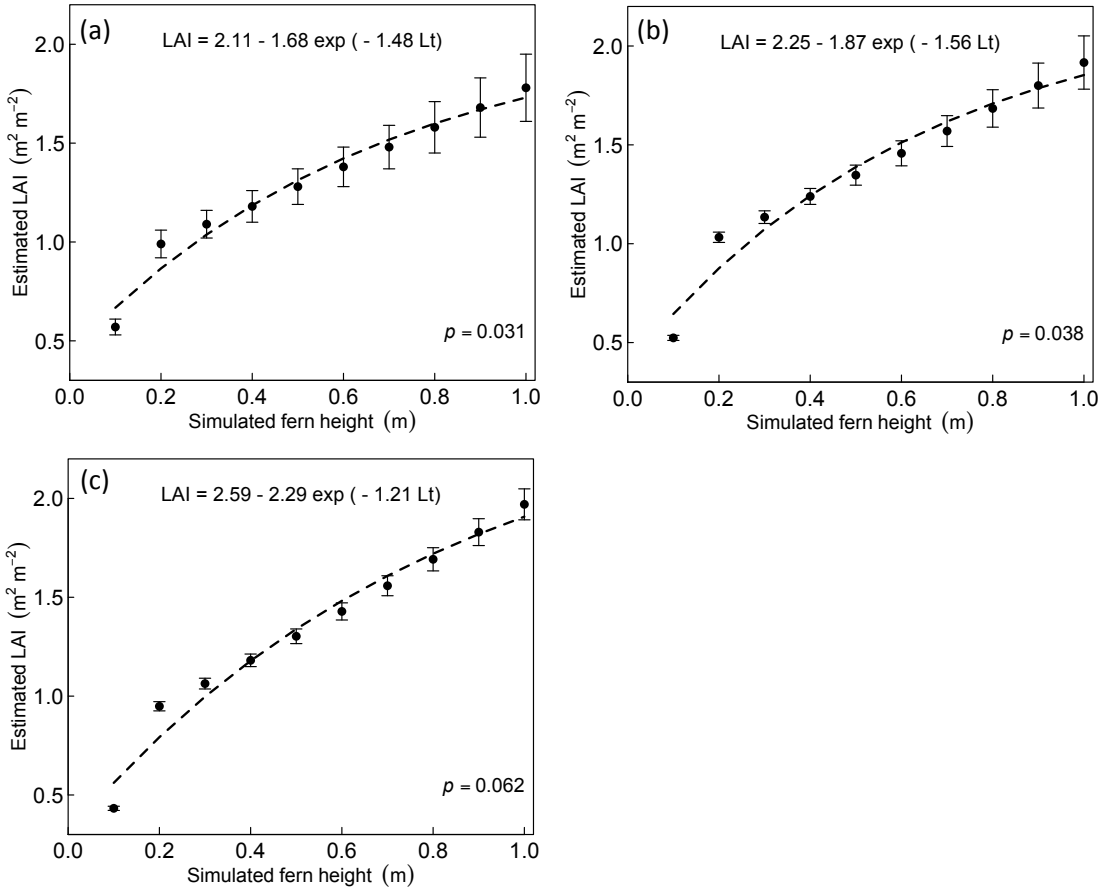

Figure 3.9. Sensitivity analysis of LAI in relation to plant height in DB site. The plant height was set from 0.1 m to 1 m with dataset of 30 May 2010 (a), 28 June 2012 (b), and 19 July 2014 (c). Vertical bars denote one standard deviation of estimated LAI.

3.4. Discussion

3.4.1. Partitioning solar radiation in the tropics

Partitioning solar radiation into VIS and the NIR components according to Weiss and Norman (1985) was parameterized using independent data sets for tropical peatland (2.3°S) in Indonesia. The parameter of η (0.55), which stand for the fraction of direct (beam) solar radiation in the visible waveband during clear- and all-sky conditions was slightly higher than values reported by Stigter and Musabilha (1982) in Tanzania (7°S). The η and the R_d/R_g (mean ± 1SD) under clear-sky conditions ($\phi < 30°$) were 0.55 ± 0.02, 0.18 ± 0.01 and 0.51 ± 0.01, 0.14 ± 0.03, respectively, for the tropical peatland and Tanzania, whereas under all sky conditions ($\phi < 30°$), their values were 0.55 ± 0.04, 0.56 ± 0.22 and 0.51 ± 0.02, 0.25 ± 0.19. In contrast, under overcast conditions ($\phi < 30°$), the η in the tropical peatland (0.56 ± 0.07) was lower than in Tanzania (0.60), with the R_d/R_g was 0.95 ± 0.02 and 1 ± 0.10, respectively for tropical peatland and Tanzania. Under all sky conditions, the R_d/R_g of tropical peatland was two times higher than Tanzania, whereas under clear sky and overcast conditions, the R_d/R_g of tropical peatland was similar to Tanzania. These indicated that the midday η was possibly larger in tropical peatland than Tanzania regardless of R_d/R_g during all conditions. The fraction of 0.55 (η), and 0.45 ($1-\eta$), respectively, for VIS and NIR components, were nearly constant throughout the years in the tropical peatland. In addition, during a clear sky condition with dominant Rayleigh scattering, the η of 0.55 in the tropical peatland is higher than in mid-latitudes (η = 0.45) (Wilson and Meyers, 2007) due to a relatively constant high solar radiation flux density in the tropics than in the mid-latitude.

3.4.2. Comparison of VIs and its seasonal variations

Our study site was located in the same area as those of Hoscilo *et al.* (2013) and Segah *et al.*, (2010). They analyzed vegetation index over the forest using SPOT-based NDVI. Similar to their results, the NDVI reached a minimum value in September-December and a maximum value in June. A comparison between satellite- and tower-based (broadband) NDVI by Segah *et al.* (2010) showed that the longevity and intensity of the 2002 drought sharply decreased the NDVI both of satellite- and tower-based measurements. However, during the wet season, broadband NDVI was relatively constant. In addition, Hoscilo *et al.* (2013) used LANDSAT TM/ETM+ NDVI for three temporal data (i.e. TM-May 1997, ETM-June 2000, and ETM-January 2003) to assess vegetation conditions, which had suffered from the different type of fires (i.e. single fire and multiple fires). Their results showed that the vegetation in their study sites recovered quickly 3 years later (2000) as the mean NDVI value of about 0.8 for both fire-suffered types sites. However, it slowly recovered, as the NDVI value of 2003 was 0.5 in the multiple fires-suffered sites (included DF and DB site). These results are comparable to our result for tower-based NDVI with a smaller inter-annual variation after the fire of 2009.

Broadband VIs agreed well to MODIS (Table 3.3), especially for the broadband NDVI. The difference in NDVI was smaller than observed for EVI2. It was lower than observed with MODIS before the fire and closely matched the MODIS after the fire. These results are similar to the results by Wilson and Meyers (2007), who found that MODIS NDVI is exceeding the broadband NDVI, with particularly large differences in the case of forest site and smaller differences in the case of grasslands and crops (note that they sampled the broadband NDVI to 16 day composites), and may result from differences in the spectral response of the sensor. In our site, the smaller difference (Fig.

3.5) between MODIS and broadband VIs in the post-fire period might be affected by an expanding oil palm plantation, which approached our site since 2011. These mixed vegetation canopy structures and the soil "background" reflectance result in a large difference in EVI2 than in NDVI because the EVI2 improved sensitivity in high biomass region while minimizing soil and atmosphere influences (Jiang *et al.*, 2008) by enhancing the VIS reflectance of a surface (Eq.3.10).

Seasonal variation of MODIS VIs slightly differed from broadband VIs. For both periods, the MODIS showed a stable distribution (May-August) with scattered values during the wet season and the latter of dry season (Fig. 3.5), owing to missing data or periods with clouds and smoke/haze in daily data. These missing data often lead to a sudden large decrease or a spike in NDVI (Wang *et al.*, 2004a). In addition, a larger footprint including mixed land-use information in data (i.e. land-cover before and after the fire observed by MODIS) with coarser spatial resolution hampered comparison to in-situ measurements, where only few trees and dominant ferns appeared in the field of view of the sensor. The broadband VIs showed clear seasonal with the peak in September/ October and a trough in April (Fig. 3.10). It mimicked seasonal variation of the NIR reflectance, as we expected that the relative seasonal amplitude of the NIR reflectance was 10 times greater than the VIS reflectance (Fig. 3.2, Fig. 3.3). Moreover, this relative amplitude was lower compared to Amazonian rainforest (Doughty and Goulden, 2008) because our site was not a dense forest in which its surface reflectance was not comparatively dark in VIS and bright in NIR reflectance.

3.4.3. Effect of peat burning on surface reflectance

This study was carried out on a burnt peat area, in which surface peat was plausible lost through large-scale fires and hence physical properties of the peat had

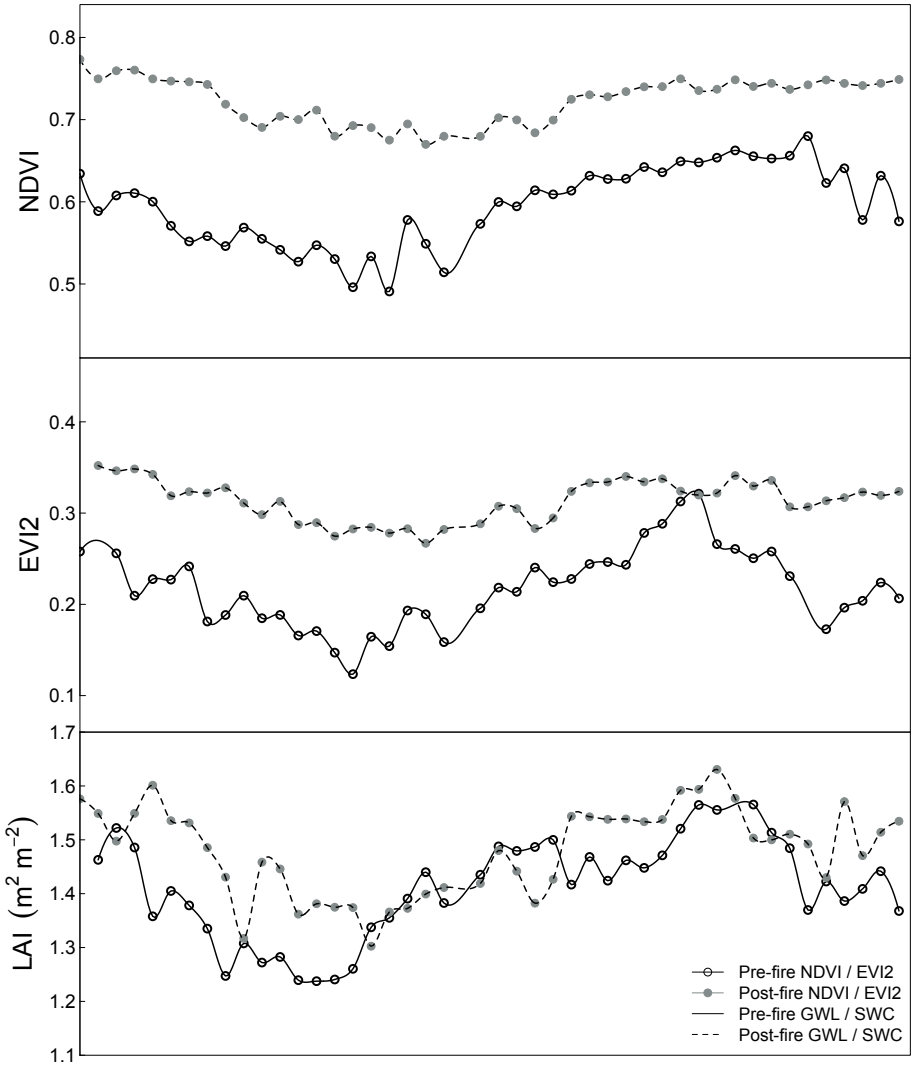

Figure 3.10 Mean seasonal variations of broadband (tower-based) NDVI, broadband (tower-based) EVI2, and leaf area index (LAI), before the fire 2009 (August 2004 – August 2009) (solid line), and after the peat fire of 2009 (December 2009 – December 2014) (dashed line). Data during the fires in 2009 and a dense smoke in 2006 were excluded.

changed after the peat fire in 2009. The loss of surface peat, which was fresher and less decomposed, and the change of surface topography with no hummocks and shallow hollow layers on the ground, increased surface runoff, and thus decreased GWL and SWC (Fig. 3.2 and Fig. 3.3). Furthermore, the conjunction of the peat fires was marked by change into a darker color and increasing fine texture on the ground. These conditions led to increased soil bulk density, hence significantly increased NIR

reflectance (Fig. 3.3). According to lab experiment on soil spectral, under wet and dry soils, the intensity of spectral reflectance in a high soil bulk density was higher than in a low bulk density because of the changes in soil structure and porosity. The high soil bulk density has a consistently high NIR reflectance with a high slope parameter for VIS reflectance (Ben-Dor *et al.*, 1997; Demattê *et al.*, 2010). Consequently, both the broadband VIs represented an overestimated value during the post-fire periods and became not reliable to reveal the change of vegetation, which was affected by the fire.

Unlike the broadband NIR reflectance, the effect of peat burning on MODIS reflectance did not significantly affect NIR MODIS (i.e. 841-876 nm) because the spectral range of about 800-900 nm in a high soil bulk density was relatively constant (Demattê *et al.*, 2010). Moreover, the MODIS with a coarser spatial resolution is not sensitive to the changes that occurred in the small areas.

3.4.4. How do LAI and VIs vary seasonally?

The in situ measurements of LAI (i.e. semi-direct method) provide a quantitative picture of fern leaf phenology in DB site (Fig. 3.7). The ferns growth (as measured by fern height) was relatively low from December through April; a period that extended through most of the wet season and flooded conditions. This low rate resulted in a relatively low and constant LAI. The leaf productions (as measured by ferns cover) and the fern height increased from April-May to July when the soil was not flooded. However, in the drier conditions, many ferns rapidly changed the leaf color into yellow or brown, and consequently, the LAI decreased rapidly during this period. The estimated LAI and broadband VIs varied seasonally in accordance with these in situ measurements. They rapidly decreased as the soil was flooded (GWL $\geq$ 0 m and SWC $\geq$ 0.62 m^3 m^{-3}), and sharply increased, as the soil was moist (GWL < 0 m and SWC $\geq$ 0.62

m^3 m^{-3}) (Fig. 3.10), especially during the pre-fire period. This implies that changing soil water availability chiefly controlled the ferns phenology at our site. Furthermore, the change in LAI closely matched with broadband EVI2 than broadband NDVI; reached a peak in September and a trough in April-May. This is due to the EVI2, which disproportionately increased the denominator of the NDVI equation relative to the VIS reflectance, thereby made the EVI2 become less sensitive to soil background.

3.4.5. Vegetation recovery in tropical peatland

The change in vegetation after the peat fire of 2009 was more clearly shown in LAI than the vegetation indices. LAI sharply decreased after the peat fire occurred. These values differed from the broadband VIs owing to the differences in surface reflectance data used. The peat fire increased the NIR-tower reflectance by a factor of two due to an increase in bulk density (section 3.4.3, Fig. 3.3), and lowered the tower VIS reflectance owing to the dark color of exposed soils and charcoal. Therefore, these conditions resulted in a separate response between LAI and broadband VIs to show vegetation recovery at DB site.

3.5. Conclusions

The ratio of photosynthetically active radiation (PAR) to global solar radiation (R_g) was relatively high in tropical peatland. Although the ratio of PAR to R_g tended to increase with the solar zenith angle, the ratio was almost constant at 0.55 at around midday regardless of R_d/R_g. This result improved a model to estimate canopy transmission and surface reflectance of solar radiation. After excluding data under dense smoke from fires, LAI varied seasonally; it decreased as the ground was flooded (GWL $\geq$ 0 m) and increased as GWL lowered underground. Before the fire of 2009, LAI

increased up to about 1.5 m^2 m^{-2} according to vegetation recovery after the fire of 2002 with the seasonal variation. The 2009 fire drastically decreased LAI, and then LAI increased year by year. Unlike the LAI, tower-based VIs showed a decreasing tendency in flooded conditions, because NIR reflectance decreased. Even after excluding data under the conditions of dense smoke and flooding, the tower-based VIs showed a different trend from MODIS-based VIs. The MODIS VIs were once decreased by the 2009 fire, and then increased according to vegetation recovery similarly with LAI, whereas tower VIs showed no decrease in 2009. This unexpected trend of tower VIs was probably caused by increased NIR reflectance due to the changed of peat bulk density because of the fire. Further field studies are needed to extract vegetation information from tower VIs by excluding the fire effect on NIR reflectance of the peat surface.

Chapter 4

General Conclusions

In this thesis, the importance of diffuse radiation for monitoring forest regrowth in tropical peatland was investigated. Special emphasis was placed on the dependence of visible (VIS) and near infrared (NIR) to diffuse radiation; the other factors that were considered as influencing the surface reflectance are the variation of groundwater levels (GWL) and soil water contents (SWC) within a sparse canopy. Analyses were performed using a model with long-term radiation data during all sky conditions, a clear sky, a moderate sky, or an overcast condition. Here, the questions raised in the introductory chapter of this thesis shall be revisited, and the answers to them obtained in the different chapters will be summarized.

- **How does the forest fires influence diffuse radiation in the tropical peat swamp forest – what is the diffuse fraction profile in tropical peatland?**

  ⇒ The answer to this question is manifold as different aspects of diffuse radiation are affected by the changes in cloud cover and atmospheric aerosol loading. Under a rainless condition with a constant value of the extra-terrestrial solar radiation (R_o) and atmospheric radiation (R_a), increasing diffuse fraction (R_d/R_g) leads to a sharp decrease in beam solar radiation (R_b) and global solar radiation

(R_g), but make an initial increase in diffuse radiation (R_d). The R_g decreased with R_d at R_d/R_g over 0.8 owing to an effect of dense aerosol loading to the atmosphere. The daily R_d/R_g was significantly related to the clearness index (R_g/R_o) with a linear threshold model. It reached its minimum of 0.51 in June (the transition between the wet and dry seasons) and its maximum of 0.68 in October (the late dry season) on a monthly basis. These patterns corresponded to the presence of precipitation owing to cloud amount. However, the pattern increased through the latter half of the dry season because of the shading by the dense smoke emitted through biomass burning and peat fires, particularly, during El Niño drought in 2002, 2006, and 2009.

- **How does severe fire affect the spectral component of solar radiation in tropical peatland?**

  ⇒ The fraction of PAR (VIS) in the tropics is strongly affected by sky conditions. In the diurnal cycle, the ratio increased in response to the R_d/R_g and solar zenith angle with its minimum of 0.54 around noon and its maximum of 0.61 around sunrise and sunset during all sky conditions. However, the midday fraction was relatively constant at 0.55 regardless of R_d/R_g during all conditions. In addition, during overcast conditions ($R_d/R_g > 0.9$ and $\phi < 70°$), the fractions (mean ± 1SD) was higher in the dry season (0.60 ± 0.21) than in the wet season (0.56 ± 0.05) because of dense smoke emitted through biomass burning and peat fires in the latter half of the dry season, particularly during El Niño years.

- **How does the surface reflectance change after forest fire in the tropical peat swamp forest – How is the vegetation recovery after fire in this ecosystem?**

⇒ The surface reflectance strongly interacts with peat's physical properties in this ecosystem. After peat fire in 2009, the surface was marked by change into a darker color with the increased fine texture on the ground. These led to increased soil bulk density, hence significantly increased NIR reflectance. This change resulted in alterations in the surface reflectance level of DB site, which was dominated by ferns with sparse canopy and little exposed bare soil. Consequently, broadband vegetation indices (VIs) represented an overestimated value during the post-fire periods and became not reliable to reveal the change of vegetation. However, the change in vegetation after the peat fire of 2009 was more clearly shown in leaf area index (LAI), sharply decreasing after the peat fire occurred. In addition, seasonal change of LAI was slightly similar to the VIs; rapidly decreased as the ground was studded with water (GWL $\geq$ 0 m) and sharply increased as GWL lowered underground.

Acknowledgments

This work would not have been possible without the assistance of many people. First of all, I would like to express my sincere gratitude to my advisor Prof Takashi Hirano for the continuous support of my Ph.D study and related research, for his guidance, insightful criticisms, and immense knowledge. Prof. Ryoji Sameshima and Dr. Tomomichi Kato for their valuable comments and suggestions during the review of this thesis. Dr. Yosuke Okimoto and Dr. Hiroyuki Yamada for their generous assistance. Dr. Hayato Tsuzuki and Dr. Tomotsugu Yazaki for providing plant-measured data and supporting data for this study, and finally Dr. Suwido Limin, Mr. Kitso Kusin, and CIMTROP team, University of Palangkaraya for their support in fieldwork and site management. I had a great time at the Laboratory of Environmental Informatics or Laboratory of Ecological and Environmental Physics, Graduate School of Agriculture, where I was heartily welcomed and want to thank my fellow labmates (former and present) for their friendly company and support during my stay in Japan. I humbly give my gratitude to the Government of Japan through the Ministry of Education, Culture, Sports, Science, and Technology (MEXT) for the scholarship (MONBUKAGAKUSHO) that enabled me to pursue my studies and being thankful to my lovely friends for informal support and encouragement.

These acknowledgments would not be complete without being grateful to my parent for being a constant source of support – emotional and moral – during my graduate years, and this thesis would certainly not have existed without them. *A special gift for my mom. Mauliate.*

Bibliography

Aldrian E, Dwi Susanto R 2003: Identification of three dominant rainfall regions within Indonesia and their relationship to sea surface temperature. Int. J. Climatol. 23, 1435 – 1452. doi:10.1002/joc.950.

Ballhorn U, Siegert F, Mason M, Limin S 2009: Derivation of burn scar depths and estimation of carbon emissions with LIDAR in Indonesian peatlands. Proc. Natl. Acad. Sci. U. S. A. 106, 21213–21218. doi:10.1073/pnas.0906457106.

Baret F, Guyot G 1991: Potentials and limits of vegetation indices for LAI and APAR assessment. Remote Sens. Environ. 35, 161 -173. doi:10.1016/0034-4257(91)90009-U.

Ben-Dor E, Inbar Y, Chen Y 1997: The reflectance spectra of organic matter in the visible near infrared and shortwave infrared region (400-2500 nm) during a controlled decomposition process. Remote Sens. Environ. 61, 1-15. doi:10.1016/S0034-4257(96)00120-4.

Berk A, Bernstein LS, Anderson GP, Acharya PK, Robertson DC, Chetwynd JH, Adler-Golden SM 1998: MODTRAN cloud and multiple scattering upgrades with application to AVIRIS. Remote Sens. Environ. 65, 367–375. doi:10.1016/S0034-4257(98)00045-5.

Bréda NJJ 2003: Ground-based measurements of leaf area index: a review of methods, instruments, and current controversies. J. Exp. Bot. 54, 2403-17. doi:10.1093/jxb/erg263.

Butt N, New M, Malhi Y, da Costa ACL, Oliveira P, Silva-Espejo JE 2010: Diffuse

radiation and cloud fraction relationships in two contrasting Amazonian rainforest sites. Agric. For. Meteorol. 150, 361–368. doi:10.1016/j.agrformet.2009.12.004.

Campbell G 1990: Derivation of an angle density function for canopies with ellipsoidal leaf angle distributions. Agric. For. Meteorol. 49, 173-176. doi:10.1016/0168-1923(90)90030-A.

Campbell G 1986: Extinction coefficients for radiation in plant canopies calculated using an ellipsoidal inclination angle distribution. Agric. For. Meteorol. 36, 317-321.doi:10.1016/0168-1923(86)90010-9.

Campbell GS, Norman JM 1998: The light environment of plant canopies. In: An Introduction to Environmental Biophysics, pp. 247–280. Springer New York, New York, NY. doi:10.1007/978-1-4612-1626-1.

Carlson TN, Ripley DA 1997: On the Relation between NDVI , Fractional Vegetation Cover , and Leaf Area Index. Remote Sens. Environ. 62, 241–242. doi:10.1016/S0034-4257(97)00104-1.

Couwenberg J, Dommain R, Joosten H 2010: Greenhouse gas fluxes from tropical peatlands in southeast Asia. Glob. Chang. Biol. 16, 1715–1732. doi:10.1111/j.1365-2486.2009.02016.x.

Demattê JAM, Nanni MR, da Silva AP, de Melo Filho JF, Dos Santos WC, Campos RC 2010: Soil density evaluated by spectral reflectance as an evidence of compaction effects. Int. J. Remote Sens. 31, 403–422. doi:10.1080/01431160902893469.

Dickinson RE 1983: Land surface process and climate – surface albedos and energy balance. Adv.Geophys. 25,305-353.

Diffendorfer J, Fleming GM, Tremor S, Spencer W, Beyers JL 2012: The role of fire severity, distance from fire perimeter and vegetation on post-fire recovery of small-mammal communities in chaparral. Int. J. Wildl. Fire. 21, 436–448. doi:10.1071/WF10060.

Disney M, Lewis P, Thackrah G, Quaife T 2004: Comparison of MODIS broadband albedo over an agricultural site with ground measurements and values derived from Earth observation data at a range of spatial scales. Int. J. Remote Sens. 25, 5927–5317. doi:10.1080/01431160410001720180.

Doughty CE, Goulden ML 2008: Seasonal patterns of tropical forest leaf area index and CO 2 exchange. J. Geophys. Res. 113, G00B06. doi:10.1029/2007JG000590.

Fan X, Chen H, Xia X, Li Z, Cribb M 2010: Aerosol optical properties from the Atmospheric Radiation Measurement Mobile Facility at Shouxian, China. J. Geophys. Res. 115, D00K33. doi:10.1029/2010JD014650.

Farquhar GD, Roderick ML 2003: Pinatubo, diffuse light, and the carbon cycle. Science. 299, 1997–1998. doi:10.1126/science.1080681.

Goudriaan J 1977: Crop Micrometeorology: a Simulation Study. Center for Agricultural Publishing and Documentation, Wageningen, the Netherlands.

Granged AJP, Jordàn A, Zavala LM, Bàrcenas G 2011: Fire-induced changes in soil water repellency increased fingered flow and runoff rates following the 2004 Huelva wildfire. Hydrol. Process. 25, 1614–1629. doi:10.1002/hyp.7923.

Gu L, Baldocchi D, Verma SB, Black TA, Vesala T, Falge EM, Dowty PR 2002: Advantages of diffuse radiation for terrestrial ecosystem productivity. J. Geophys. Res. 107. doi:10.1029/2001JD001242.

Heil A, Langmann B, Aldrian E 2007: Indonesian peat and vegetation fire emissions: Study on factors influencing large-scale smoke haze pollution using a regional atmospheric chemistry model. Mitig. Adapt. Strateg. Glob. Chang. 12, 113–133. doi:10.1007/s11027-006-9045-6.

Hirano T, Kusin K, Limin S, Osaki M 2015: Evapotranspiration of tropical peat swamp forests. Glob. Chang. Biol. 21, 1914–1927. doi:10.1111/gcb.12653.

Hirano T, Kusin K, Limin S, Osaki M 2014: Carbon dioxide emissions through oxidative

peat decomposition on a burnt tropical peatland. Glob. Chang. Biol. 20, 555–65. doi:10.1111/gcb.12296.

Hirano T, Segah H, Harada T, Limin S, June T, Hirata R, Osaki M 2007: Carbon dioxide balance of a tropical peat swamp forest in Kalimantan, Indonesia. Glob. Chang. Biol. 13, 412–425. doi:10.1111/j.1365-2486.2006.01301.x.

Hirano T, Segah H, Kusin K, Limin S, Takahashi H, Osaki M 2012: Effects of disturbances on the carbon balance of tropical peat swamp forests. Glob. Chang. Biol. 18, 3410–3422. doi:10.1111/j.1365-2486.2012.02793.x.

Hooijer A, Page S, Canadell JG, Silvius M, Kwadijk J, Wosten H, Jauhiainen J 2010: Current and future CO_2 emissions from drained peatlands in Southeast Asia. Biogeosciences. 7, 1505–1514. doi:10.5194/bg-7-1505-2010.

Hoscilo A, Page SE, Tansey KJ, Rieley JO 2011: Effect of repeated fires on land-cover change on peatland in southern Central Kalimantan, Indonesia, from 1973 to 2005. Int. J. Wildl. Fire 20, 578–588. doi:10.1071/WF10029.

Hoscilo A, Tansey KJ, Page SE 2013: Post-fire vegetation response as a proxy to quantify the magnitude of burn severity in tropical peatland. Int. J. Remote Sens. 34, 412–433. doi:10.1080/01431161.2012.709328.

Huemmrich KF, Black TA, Jarvis PG, McCaughey JH, Hall FG 1999: High temporal resolution NDVI phenology from micrometeorological radiation sensors. J. Geophys. Res. 104, 27935. doi:10.1029/1999JD900164.

Ikegami M, Okada K, Zaizen Y, Makino Y, Jensen JB, Gras JL, Harjanto H 2001: Very high weight ratios of S/K in individual haze particles over Kalimantan during the 1997 Indonesian forest fires. Atmos. Environ. 35, 4237–4243. doi:10.1016/S1352-2310(01)00247-3.

Jenkins JP, Richardson AD, Braswell BH, Ollinger SV, Hollinger DY, Smith ML 2007: Refining light-use efficiency calculations for a deciduous forest canopy using simultaneous tower-based carbon flux and radiometric measurements. Agric. For.

Meteorol. 143, 64–79. doi:10.1016/j.agrformet.2006.11.008.

Jiang Z, Huete AR, Didan K, Miura T 2008: Development of a two-band enhanced vegetation index without a blue band. Remote Sens. Environ. 112, 3833–3845. doi:10.1016/j.rse.2008.06.006.

Jordán A, Zavala LM, Mataix-Solera J, Nava AL, Alanís N 2011: Catena Effect of fire severity on water repellency and aggregate stability on Mexican volcanic soils. Catena 84, 136–147. doi:10.1016/j.catena.2010.10.007.

Kanniah KD, Beringer J, North P, Hutley L 2012: Control of atmospheric particles on diffuse radiation and terrestrial plant productivity: A review. Prog. Phys. Geogr. 36, 209–237. doi:10.1177/0309133311434244.

Kaufman YJ, Fraser RS 1997: The effect of smoke particles effect on clouds and climate forcing. Science. 277, 1636–1639. doi: 10.1126/science.277.5332.1636

Khan BH 2009: Solar energy – basics. In: Non-Conventional Energy Resources, pp. 82-115. Tata McGraw Hill Education Private Limited, New Delhi.

Knohl A, Baldocchi DD 2008: Effects of diffuse radiation on canopy gas exchange processes in a forest ecosystem. J. Geophys. Res. 113, G02023. doi:10.1029/2007JG000663.

Knox KJE, Clarke PJ 2006: Fire season and intensity affect shrub recruitment in temperate sclerophyllous woodlands. Oecologia. 149, 730–739. doi:10.1007/s00442-006-0480-6.

Konstantinidis P, Tsiourlis G, Xofis P 2006: Effect of fire season, aspect, and pre-fire plant size on the growth of Arbutus unedo L. (strawberry tree) resprouts. For. Ecol. Manage. 225, 359–367. doi:10.1016/j.foreco.2006.01.011.

Kuenzi AM, Fule PZ, Sieg CH 2008: Effects of fire severity and pre-fire stand treatment on plant community recovery after a large wildfire. For. Ecol. Manage. 255, 855–865. doi:10.1016/j.foreco.2007.10.001.

Kume T, Tanaka N, Kuraji K, Komatsu H, Yoshifuji N, Saitoh TM, Suzuki M, Kumagai T 2011: Ten-year evapotranspiration estimates in a Bornean tropical rainforest. Agric.

For. Meteorol. 151, 1183–1192. doi:10.1016/j.agrformet.2011.04.005.

Langner A, Siegert F 2009: Spatiotemporal fire occurrence in Borneo over a period of 10 years. Glob. Chang. Biol. 15, 48–62. doi:10.1111/j.1365-2486.2008.01828.x.

Lewis SL 2006: Tropical forests and the changing earth system. Philos. Trans. R. Soc. Lond. B. Biol. Sci. 361, 195–210. doi:10.1098/rstb.2005.1711.

Marpaung F, Hirano T 2014: Environmental dependence and seasonal variation of diffuse solar radiation in tropical peatland. J. Agric. Meteorol. 70, 334–341. doi:10.2480/agrmet.D-14-00028.

Mataix-Solera J, Cerdà A, Arcenegui V, Jordán A, Zavala LM 2011: Earth-Science Reviews Fire effects on soil aggregation : A review. Earth Sci. Rev. 109, 44–60. doi:10.1016/j.earscirev.2011.08.002.

Matsui T, Beltrán-Przekurat A, Niyogi D, Pielke RA, Coughenour M 2008: Aerosol light scattering effect on terrestrial plant productivity and energy fluxes over the eastern United States. J. Geophys. Res. 113, D14S14. doi:10.1029/2007JD009658.

Mercado LM, Bellouin N, Sitch S, Boucher O, Huntingford C, Wild M, Cox PM 2009: Impact of changes in diffuse radiation on the global land carbon sink. Nature 458, 1014–7. doi:10.1038/nature07949.

Miettinen J, Liew SC 2010: Degradation and development of peatlands in Peninsular Malaysia and in the islands of Sumatra and Borneo since 1990. L. Degrad. Dev. 21, 285–296. doi:10.1002/ldr.976.

Miettinen J, Shi C, Liew SC 2011: Deforestation rates in insular Southeast Asia between 2000 and 2010. Glob. Chang. Biol. 17, 2261–2270. doi:10.1111/j.1365-2486.2011.02398.x.

Monteith JL, Unsworth MH 2013: Principles of Environmental Physics Plants, Animals, and the Atmosphere, Fourth. ed. Elsevier Ltd. doi:10.1016/B978-0-12-386910-4.00019-6.

Murdiyarso D, Adiningsih ES 2007: Climate anomalies, Indonesian vegetation fires, and terrestrial carbon emissions. Mitig. Adapt. Strateg. Glob. Chang. 12, 101–112. doi:10.1007/s11027-006-9047-4.

Myneni RB, Keeling CD, Tucker CJ, Asrar G, Nemani RR 1997: Increased plant growth in the northern high latitudes from 1981 to 1991. Nature. doi:10.1038/386698a0.

Nagai S, Ishii R, Suhaili A. Bin Kobayashi H, Matsuoka M, Ichie T, Motohka T, Kendawang JJ, Suzuki R 2014: Usability of noise-free daily satellite-observed green–red vegetation index values for monitoring ecosystem changes in Borneo. Int. J. Remote Sens. 35, 7910–7926. doi:10.1080/01431161.2014.978039.

Norman JM 1979: Modeling the complete crop canopy. In modification of the aerial environment of crops (eds. B.J. Barfiled and J. Gerber), American Society of Agricultural Engineers, St. Joseph, MI. 149-177.

Nagai S, Saigusa N, Muraoka H, Nasahara KN 2009: What makes the satellite-based EVI–GPP relationship unclear in a deciduous broad-leaved forest? Ecol. Res. 25, 359–365. doi:10.1007/s11284-009-0663-9.

Oak Ridge National Laboratory Distributed Active Archive Center (ORNL DAAC) 2015: MODIS subsetted land products, Collection 5. Available on-line [http://daac.ornl.gov/MODIS/modis.html] from ORNL DAAC, Oak Ridge, Tennessee, U.S.A. Subset obtained for MOD09A1 product at 2.341S,114.038E, time period: 2004-04-14 to 2014-12-27.

Oldeman LR, Las I, Muladi 1980: The agroclimatic maps of Kalimantan, Maluku, Irian Jaya and Bali, West and East Nusa Tenggara, pp.1-32. Central Research Institute for Agriculture, Bogor.

Oliphant AJ, Dragoni D, Deng B, Grimmond CSB, Schmid HP, Scott SL 2011: The role of sky conditions on gross primary production in a mixed deciduous forest. Agric. For. Meteorol. 151, 781–791. doi:10.1016/j.agrformet.2011.01.005.

Oliveira PHF, Artaxo P, Pires C, de Lucca S, Procópio A, Holben B, Schafer J, Cardoso LF,

Wofsy SC, Rocha HR 2007: The effects of biomass burning aerosols and clouds on the CO 2 flux in Amazonia. Tellus B. 59, 338–349. doi:10.1111/j.1600-0889.2007.00270.x.

Page SE, Rieley JO, Banks CJ 2011: Global and regional importance of the tropical peatland carbon pool. Glob. Chang. Biol. 17, 798–818. doi:10.1111/j.1365-2486.2010.02279.x.

Page SE, Siegert F, Rieley JO, Boehm HD, Jaya A, Limin S 2002: The amount of carbon released from peat and forest fires in Indonesia during 1997. Nature. 420, 61–66. doi:10.1038/nature01141.1.

Pavlovic NB, Leicht-Young SA, Grundel R 2011: Short-term effects of burn season on flowering phenology of savanna plants. Plant Ecol. doi:10.1007/s11258-010-9851-5.

Pereira P, Úbeda X, Martin DA 2012: Fire severity effects on ash chemical composition and water-extractable elements. Geoderma. 212, 611–625. doi:10.1016/j.geoderma.2012.02.005.

Putra EI, Hayasaka H 2011: The effect of the precipitation pattern of the dry season on peat fire occurrence in the Mega Rice Project area, Central Kalimantan, Indonesia. Tropics. 19, 145–156. doi:10.3759/tropics.19.145.

Putra EI, Hayasaka H, Takahashi H, Usup A 2008: Recent Peat Fire Activity in the Mega Rice Project Area , Central Kalimantan , Indonesia. J. Disaster Res. 3, 334–341.

Ramanathan V, Crutzen PJ, Lelieveld J et al. 2001: Indian Ocean Experiment: An integrated analysis of the climate forcing and effects of the great Indo-Asian haze. J. Geophys. Res. Atmos. 106, 28371–28398. doi:10.1029/2001JD900133.

Roderick M, Farquhar G, Berry S, Noble I 2001: On the direct effect of clouds and atmospheric particles on the productivity and structure of vegetation. Oecologia. 129, 21–30. doi:10.1007/s004420100760.

Roderick ML 1999: Estimating the diffuse component from daily and monthly

measurements of global radiation. Agric. For. Meteorol. 95, 169–185. doi:10.1016/S0168-1923(99)00028-3.

Ross J 1981: Tasks for vegetation science 3. Dr W Junk Publishers, The Hague, The Netherlands. doi:978-94-009-8649-7.

Ross J, Sulev M 2000: Sources of errors in measurements of PAR. Agric. For. Meteorol. 100, 103–125. doi:10.1016/S0168-1923(99)00144-6.

Segah H, Tani H, Hirano T 2010: Detection of fire impact and vegetation recovery over tropical peat swamp forest by satellite data and ground-based NDVI instrument. Int. J. Remote Sens. doi:10.1080/01431160903302981.

Sorensen KW 1993: Indonesian peat swamp forests and their role as a carbon sink. Chemosphere. 27, 1065–1082. doi:10.1016/0045-6535(93)90068-G.

Spitters CJT 1986: Separating the diffuse and direct component of global radiation and its implications for modeling canopy photosynthesis Part II. Calculation of canopy photosynthesis. Agric. For. Meteorol. 38, 231–242. doi:10.1016/0168-1923(86)90061-4.

Spitters CJT, Toussaint HAJM, Goudriaan J 1986: Separating the diffuse and direct component of global radiation and its implications for modeling canopy photosynthesis Part I. Components of incoming radiation. Agric. For. Meteorol. 38, 217–229. doi:10.1016/0168-1923(86)90060-2.

Steltzer H, Welker JM 2006: Modeling the effect of photosynthetic vegetation properties on the NDVI-LAI relationship. Ecology. 87, 2765–2772. doi:10.1890/0012-9658(2006)87[2765:MTEOPV]2.0.CO;2.

Stigter C, Musabilha VM 1982: The conservative ratio of photosynthetically active to total radiation in the tropics. J. Appl. Ecol. 19, 853–858. doi:10.2307/2403287.

Still CJ, Riley WJ, Biraud SC et al. 2009: Influence of clouds and diffuse radiation on ecosystem-atmosphere CO_2 and $CO^{18}O$ exchanges. J. Geophys. Res. 114, G01018.

doi:10.1029/2007JG000675.

Sundari S, Hirano T, Yamada H, Kusin K, Limin S 2012: Effect of groundwater level on soil respiration in tropical peat swamp forests. J. Agric. Meteorol. 68, 121–134. doi:10.2480/agrmet.68.2.6.

Suzaki T, Kume A, Ino Y 2003: Evaluation of direct and diffuse radiation densities under forest canopies and validation of the light diffusion effect. J. For. Res. 8, 283–290. doi:10.1007/s10310-003-0038-y.

Tansey K, Beston J, Hoscilo A, Page SE, Paredes Hernández CU 2008: Relationship between MODIS fire hot spot count and burned area in a degraded tropical peat swamp forest in Central Kalimantan, Indonesia. J. Geophys. Res. 113, D23112. doi:10.1029/2008JD010717.

Tessler N, Sapir Y, Wittenberg L, Greenbaum N 2015: Recovery of Mediterranean Vegetation after Recurrent Forest Fires: Insight from the 2010 Forest Fire on Mount Carmel, Israel. L. Degrad. Dev. doi:10.1002/ldr.2419.

Toriyama J, Takahashi T, Nishimura S at al. 2014: Estimation of fuel mass and its loss during a forest fire in peat swamp forests of Central Kalimantan, Indonesia. For. Ecol. Manage. 314, 1–8. doi:10.1016/j.foreco.2013.11.034.

Tosca MG, Randerson JT, Zender CS, Nelson DL, Diner DJ, Logan JA 2011: Dynamics of fire plumes and smoke clouds associated with peat and deforestation fires in Indonesia. J. Geophys. Res. Atmos. 116, 1–14. doi:10.1029/2010JD015148.

Tucker CJ 1979: Red and photographic infrared linear combinations for monitoring vegetation. Remote Sens. Environ. 150, 127–150. doi:10.1016/0034-4257(79)90013-0.

Tucker CJ, Sellers PJ 1986: Satellite remote sensing of primary production. Int. J. Remote Sens. 7, 1395–1416. doi:10.1080/01431168608948944.

Turner DP, Ollinger SV, Kimball JS 2004: Integrating Remote Sensing and Ecosystem Process Models for Landscape- to Regional-Scale Analysis of the Carbon Cycle.

Bioscience. 54, 573. doi:10.1641/0006-3568(2004)054[0573:IRSAEP]2.0.CO;2.

van der Werf GR, Dempewolf J, Trigg SN et al. 2008: Climate regulation of fire emissions and deforestation in equatorial Asia. Proc. Natl. Acad. Sci. U.S.A. 105, 20350–5. doi:10.1073/pnas. 0803375105.

Verstraete MM, Pinty B 1996: Designing optimal spectral indexes for remote sensing applications. IEEE Trans. Geosci. Remote Sens. 34, 1254–1265. doi:10.1109/36.536541.

Vivian LM, Cary GJ, Bradstock RA, Gill AM 2008: Influence of fire severity on the regeneration , recruitment and distribution of eucalypts in the Cotter River Catchment , Australian Capital Territory. Austral Ecol. 33, 55–67. doi:10.1111/j.1442-9993.2007.01790.x.

Wang Q, Tenhunen J, Dinh NQ, Reichstein M, Vesala T, Keronen P 2004a: Similarities in ground- and satellite-based NDVI time series and their relationship to physiological activity of a Scots pine forest in Finland. Remote Sens. Environ. doi:10.1016/j.rse.2004.07.006.

Wang Q, Tenhunen J, Granier A, Reichstein M, Bouriaud O, Nguyen D, Breda N 2004b: Long-term variations in leaf area index and light extinction in a Fagus sylvatica stand as estimated from global radiation profiles. Theor. Appl. Climatol. 93, 225–237. doi:10.1007/s00704-004-0074-3.

Wang WC 1976: A parameterization for the absorption of solar radiation by water vapor in the earth's atmosphere. J. Appl. Meteorol. 21–27. doi:10.1175/1520-0450(1976) 015<0021:APFTAO>2.0.CO;2.

Weiss A, Norman JM 1985: Partitioning solar radiation into direct and diffuse, visible and near-infrared components. Agric. For. Meteorol. 34, 205–213. doi:10.1016/0168-1923(85)90020-6.

Wilson TB, Meyers TP 2007: Determining vegetation indices from solar and photosynthetically active radiation fluxes. Agric. For. Meteorol. 144, 160–179.

doi:10.1016/j.agrformet.2007.04.001.

Yulianti N, Hayasaka H, Usup A 2012: Recent Forest and Peat Fire Trends in Indonesia The Latest Decade by MODIS Hotspot Data. Glob. Environ. Res. 16, 105–116.

Zhang M, Yu GR, Zhuang J et al. 2011: Effects of cloudiness change on net ecosystem exchange, light use efficiency, and water use efficiency in typical ecosystems of China. Agric. For. Meteorol. 151, 803–816. doi:10.1016/j.agrformet.2011.01.011.